Copernicus Marine Service

QUALITY INFORMATION DOCUMENT

Black Sea MFC

BLKSEA_MULTIYEAR_WAV_007_006

Issue: 3.1

Contributors: Joanna Staneva, Marcel Ricker, Arno Behrens

Approval date by the CMEMS product quality coordination team: 23/11/2023

CHANGE RECORD

When the quality of the products changes, the QuID is updated and a row is added to this table. The third column specifies which sections or sub-sections have been updated. The fourth column should mention the version of the product to which the change applies.

Issue	Date	§	Description of Change	Author	Validated By
1.0	01/09/2019	All	First version of document of CMEMS V4	J. Staneva, A. Behrens, G. Gayer,	E. Peneva
2.0	07/12/2020	All	Complete revision due to new model version	J. Staneva, A. Behrens, M. Ricker,	E. Peneva
2.1	15/01/2021	§I, §VI	Addition of the interim dataset	J. Staneva, A. Behrens	E. Peneva
2.2	10/09/2021	§VI	Addition of the 2020 time series extension	J. Staneva, M. Ricker, A. Behrens	E. Peneva
3.0	29/11/2022	All	Complete revision due to new model version	J. Staneva, M. Ricker, A. Behrens	E. Peneva
3.1	30/11/2023	All	Addition of time series extension to 1950 and addition of LATEMAR max. variables	J. Staneva, M. Ricker, A. Behrens	E. Peneva

TABLE OF CONTENTS

Applicable and Reference Documents

	Ref	Title	Date / Version
[DA1]	CMEMS-BS-PUM-007-006	Black Sea Waves Reanalysis Product User Manual	Nov 2023 / 3.1

I EXECUTIVE SUMMARY

I.1 Products covered by this document

This document describes the quality of the new Multi-Year Product (MYP) for the Black Sea wave component (BLKSEA_MULTIYEAR_WAV_007_006). The BS-wave product includes the complete hindcast time period 01/01/1950 – 31/12/2022. The product includes the following 2D 1-hourly analysis and forecast instantaneous fields:

- VHMO: spectral significant wave height (Hm0);
- VTM10: spectral moments (-1,0) wave period (Tm-10);
- VTM02: spectral moments (0,2) wave period (Tm02);
- VTPK: wave period at spectral peak / peak period (Tp);
- VMDR: mean wave direction from (Mdir);
- VPED: wave principal direction at spectral peak;
- VSDX: stokes drift U;
- VSDY: stokes drift V;
- VHM0_WW: spectral significant wind wave height;
- VTM01_WW: spectral moments (0,1) wind wave period;
- VMDR_SW1: mean wind wave direction from;
- VHM0_SW1: spectral significant primary swell wave height;
- VTM01_SW1: spectral moments (0,1) primary swell wave period;
- VMDR_SW1: mean primary swell wave direction from;
- VHM0_SW2: spectral significant secondary swell wave height;
- VTM01_SW2: spectral moments (0,1) secondary swell wave period;
- VMDR_SW2: mean secondary swell wave direction from;
- VCMX: maximum crest trough wave height (Hc,max); and
- VMXL: height of the highest crest.

The output data are produced at 1/40°x1/40° horizontal resolution.

Interim datasets are also provided: they consist of operational datasets that will be updated every month M to cover the month M-1 and produced by the BS-Wave MY system, forced by ECMWF ERA5 atmospheric fields. Details on the processing system are provided in [DA1].

I.2 Summary of the results

The quality of the MYP BLKSEA_MULTIYEAR_WAV_007_006 has been assessed via comparing the reanalyses against satellite observations recorded by the radar altimeters of Jason-1, Jason-2 and Jason-3, for the time period from 01/01/2002 to 31/12/2021, independent not assimilated satellite data, and available in-situ observations. For the time period from 01/01/1950 to 31/12/2001 no satellite measurements were available to compare with. The horizontal spatial grid resolution of the BS-waves model is 1/40° in zonal direction and 1/40° in meridional direction (ca. 2.5 km).

The main results of the BLKSEA_MULTIYEAR_WAV_007_006 quality product assessment are summarized below:

Significant wave height: The comparisons of the significant wave height (SWH) have been done with satellite altimeter data (assimilated and non-assimilated data) for the time period from 2002 to 2021 and in-situ observations. The V4 BS-waves system used to produce the product BLKSEA_MULTIYEAR_WAV_007_006 presents good accuracy in terms of the SWH. The model skill enhancement based on different statistical parameters compared to the old product is evident. The model skill enhancement is mainly related to a reduced bias and reduced differences between model and satellite data. The skills critically depend upon the quality and the temporal and spatial resolution of the wind forcing for the Black Sea. The newly introduced wind assessments reveal good wind data quality with underestimated high wind speeds. However, significant wave heights show no distinct deviation from the measurements over the full range of wave heights. In total, the wave model results and observations are correlated at a level of 0.92 or better. In general, the wave model tends to slightly overestimate the satellite measurements. The bias (mean of the difference model minus measurements) is always very small with values between -0.01 and 0.03 m. It is also noteworthy that BLKSEA_MULTIYEAR_WAV_007_006 SWH product can capture the temporal variability very well for almost all parts of the distribution of significant wave heights.

Wave Buoy validations: In the period May 2020 to December 2021 time series of eleven buoys (SPOT0772, SPOT0773, SPOT0776, WAVEB01, WAVEB02, WAVEB03, WAVEB04, WAVEB05, WAVEB06, WD3044, Gelendzhik) were available (INSITU_BS_NRT_OBSERVATIONS_013_034). The water depth at the buoy locations is often shallow (17 m/20 m) and the wave buoys are located close to the coast. The quality control of some of the stations is still insufficient, which limits the validations against in-situ observations. Nevertheless, the modelled significant wave height shows a good correlation with buoy data. In addition to SWH, the in-situ observations provide other wave parameters, such as maximum wave height, mean direction, peak direction, T_{M02} period, and peak period. The correlation between the model and buoy data for these parameters is also very good. Some peaks of the SWH in the time series are slightly underestimated compared to in-situ observations. Reasons for this could be the vicinity of the coast, the model resolution or deviations in the bathymetry from the real water depth. In the future, buoy data for past periods will be collected and implemented into the quality control in order to assess past periods of the dataset.

I.3 Estimated Accuracy Numbers

Estimated Accuracy Numbers (EANs) for the results of the BS-waves reanalysis are the mean of the differences between measured and computed values (bias) and the corresponding root mean square differences (RMSD).

EANs are computed for:

- Significant Wave Height (SWH): Refers to the "spectral significant wave height (VHM0)".

The observations are:

- Significant wave heights (assimilated): recorded by the radar altimeters of the satellites Jason-1 (JS1), Jason-2 (JS2), and Jason-3 (JS3) that are available on the public server of AVISO (ftp-access.aviso.altimetry.fr), which additionally include wind speed measurements. These data have also been merged and hereafter named JSall.
- Significant wave heights (not assimilated): recorded by the radar altimeters of the satellites Sentinel-3a/-3b (NRT), HaiYang-2b (NRT), Cryosat-2 (NRT+MY), CFOSat (NRT+MY), Saral/Altika

(NRT+MY), and Envisat (MY). These data taken from the CMEMS NRT and MY wave altimeter datasets. These data have been merged and hereafter named All merged.
- Significant wave height: recorded by the available wave buoys for the considered period.
- Significant wave height and peak period: recorded by the ADCP station Pasha Dere located at 28.03 °E, 43.08 °N.

The EANS computed for the V4 version of the CMEMS Black Sea wave modelling system are based on the simulation of the system in hindcast mode for 20 years (January 2002 – December 2021) of the complete hindcast period (January 1950 – December 2022). For the first 52 years between January 1950 and December 2001 there are no measurements available to compare with. Concerning the lack of systematic in-situ measurements in the Black Sea, satellite measurements are the major source to compare the wave model results. The final values for BIAS and RMSD (common nomenclature of these metrics in the literature on wave modelling) are given in Table 1 for each of the three satellites spanning different periods and for the case when all satellite measurements are combined. Since the BIAS is the difference for the model mean minus the mean of the measurements, the EANs for the BS-waves system indicate a very slight underestimation of the measurements by the wave model, especially for the comparisons with the Jason-3 data. In addition, to evaluate an expected improvement of the new model version, section VII compares the old model skills to the new one.

Table 1: EANs for the BLKSEA_MULTIYEAR_WAV_007_006 reanalysis (all values in centimetres).

2002-2013 (Jason-1)		**2008-2019 (Jason-2)**		**2016-2021 (Jason-3)**		**2002-2021 (combined)**	
Bias [cm]	RMSD	bias [cm]	RMSD	bias [cm]	RMSD[cm]	bias [cm]	RMSD
3	19	1	25	-1	25	2	23

II PRODUCTION SYSTEM DESCRIPTION

II.1 Production centre details

Production centre name: Helmholtz-Zentrum Hereon (former HZG), Germany

Production system name: Black Sea Waves Reanalysis

Available variables (2D):

- VHMO: spectral significant wave height (Hm0);
- VTM10: spectral moments (-1,0) wave period (Tm-10);
- VTM02: spectral moments (0,2) wave period (Tm02);
- VTPK: wave period at spectral peak / peak period (Tp);
- VMDR: mean wave direction from (Mdir);
- VPED: wave principal direction at spectral peak;
- VSDX: stokes drift U;
- VSDY: stokes drift V;
- VHM0_WW: spectral significant wind wave height;
- VTM01_WW: spectral moments (0,1) wind wave period;
- VMDR_SW1: mean wind wave direction from;
- VHM0_SW1: spectral significant primary swell wave height;
- VTM01_SW1: spectral moments (0,1) primary swell wave period;
- VMDR_SW1: mean primary swell wave direction from;
- VHM0_SW2: spectral significant secondary swell wave height;
- VTM01_SW2: spectral moments (0,1) secondary swell wave period;
- VMDR_SW2: mean secondary swell wave direction from;
- VCMX: maximum crest trough wave height (Hc,max); and
- VMXL: height of the highest crest.

Frequency of model output: Hourly instantaneous

Geographical coverage: 27.25°E → 42.00°E; 40.50°N → 47.00°N (the Azov Sea is excluded)

Horizontal resolution: 1/40° in zonal direction, 1/40° in meridional direction (ca. 2.5 km)

Vertical coverage: Surface only

Frequency of hindcast release: Reanalysis: once a year, Interim: monthly

Data assimilation: Yes, significant wave height and wind speed data from the satellites Jason-1, Jason-2, and Jason-3 (from AVISO).

Citation (DOI): Staneva, J., Ricker, M., & Behrens, A. (2022). Black Sea Waves Reanalysis (CMEMS BS-Waves, EAS4 system) (Version 1) [Data set]. Copernicus Monitoring Environment Marine Service (CMEMS). https://doi.org/10.25423/CMCC/BLKSEA_MULTIYEAR_WAV_007_006_EAS4

The wave reanalysis for the Black Sea are produced by the Hereon Production Unit utilizing the wave model WAM (described below).

The BS-waves system integration is composed of several steps:

1. Upstream data acquisition, pre-processing and control of: ECMWF (European Centre for Medium-Range Weather Forecasts) ERA-5 (atmospheric reanalysis) atmospheric forcing in an one-hourly temporal and 0.25° lateral resolution and of the AVISO satellite data.
2. Hindcast: WAM produces BLKSEA_MULTIYEAR_WAV_007_006.
3. Post processing: the model output is processed to obtain the products for the CMEMS catalogue.
4. Output delivery.

The BLKSEA_MULTIYEAR_WAV_007_006 production chain is represented in Figure 1.

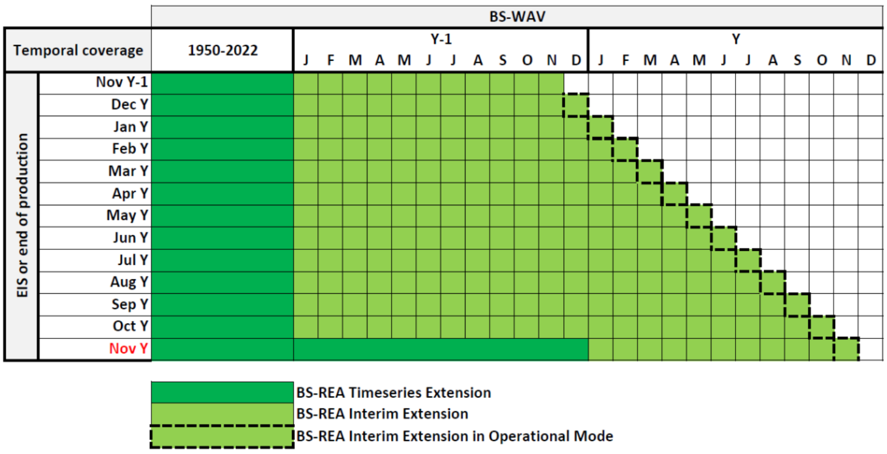

Figure 1: BS-WAV production chain.

Commented [MR1]: Updated

II.2 System Description

This document details the quality of products from the Black Sea Wave Reanalysis system. These products are generated using the WAM Cycle 6 Black Sea model with a spatial resolution of about 2.5 km, which became operational within CMEMS in April 2020 and was subsequently used to produce the BLKSEA_MULTIYEAR_WAV_007_006 reanalysis. The wave model describes ocean surface gravity wave (periods 1.5 to 24 seconds) characteristics as an extension to the existing physical and ecosystem model products provided by the Black Sea MFC. The following subsections describe the model component and its dependencies in terms of models providing the forcing.

Region, grid and bathymetry

The regional wave model for the semi-enclosed Black Sea runs in deep water mode on a model grid situated between 27.25°E to 42.00°E and 40.50°N to 47.00°N, with a spatial resolution of about 2.5 km, (1/40° in latitude and longitude direction). The required bathymetry for the model grid is based upon the General Bathymetric Chart of the Oceans (GEBCO 2019 Grid, http://www.gebco.net) 30 *sec* data. The bathymetry is only a controlling mechanism on the wave field for depths below approximately 490 m, based on a minimum frequency in the model of 0.042 Hz (period 24 seconds). The model area and the corresponding depth distribution are shown in Figure 2.

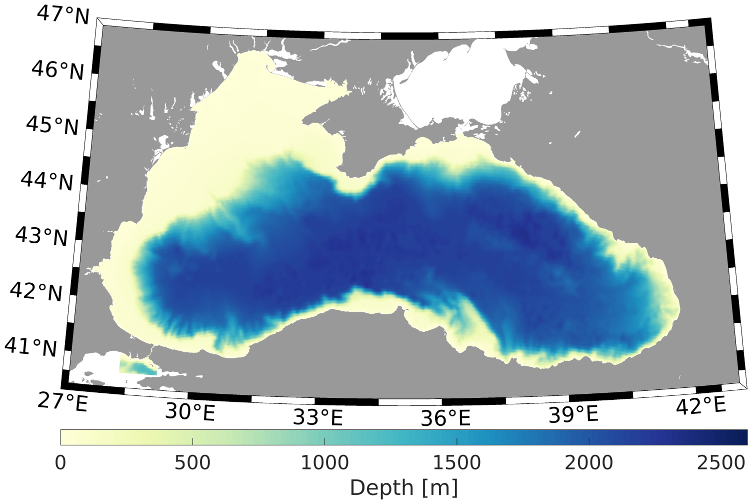

Figure 2: Black Sea wave model WAM bathymetry.

Spectral grid

WAM calculates the two-dimensional energy density spectrum at each of the 74,518 active model grid points in the frequency and directional space. The solution of the energy balance equation is provided for 24 directional bands at 15° each, starting at 7.5° and measured clockwise with respect to true north, and 30 frequencies logarithmically spaced from 0.042 Hz to 0.663 Hz at intervals of $\Delta f/f = 0.1$. Therefore, the prognostic part of the wave model covers periods from approximately 23.8 to 1.5 seconds. In order to include the important contribution of higher frequency waves to wave growth/dissipation processes and for the output wave characteristics a parametric tail is fitted for frequencies above the spectral maximum (e.g. WAMDI Group, 1988).

Wave model and source term physics configuration

The system BS-waves is based on the state-of-the-art and well-established advanced third-generation spectral wave model WAM that runs successfully at many institutions worldwide. It is based on the spectral description of the wave conditions in frequency and directional space at each of the active model sea grid points of a certain model area. The energy balance equation, complemented with a suitable description of the relevant physical processes is used to follow the evolution of each wave spectral component. WAM computes the two-dimensional wave variance spectrum through the integration of the transport equation (1) in spherical coordinates (see also ECMWF (2020)):

$$\frac{\partial F}{\partial t} + (\cos\Phi)^{-1}\frac{\partial}{\partial\Phi}(\Phi\cos\Phi F) + \frac{\partial}{\partial\lambda}(\lambda F) + \sigma\frac{\partial}{\partial\sigma}\left(\sigma\frac{F}{\sigma}\right) + \frac{\partial}{\partial\theta}(\theta F) = S \tag{1}$$

$$\dot{\Phi} = (c_g \cos\theta + u_{North})/R$$

$$\dot{\lambda} = (c_g \sin\theta + u_{East})/(R\cos\Phi)$$

$$\dot{\theta} = c_g \sin\theta \tan\Phi/\mathrm{R} + \dot{\theta}_D + \dot{\theta}_C$$

$$\dot{\sigma} = \sigma_C$$

with,

$\mathrm{F}(\lambda, \Phi, \sigma, \theta, \mathrm{t})$	wave energy density spectrum
(λ, Φ)	longitude, latitude
(σ, θ)	intrinsic frequency, wave direction

The first term of (1) describes the local rate of change of energy density in time, the second and third ones the propagation in geographical space, the fourth one the shifting of the relative frequency due to variations in depths and currents and the last one on the left side of the equation the contribution of the depth- and current-induced refraction. The source functions on the right of the transport equation comprise the contributions of wind input (S_{in}), nonlinear interaction (S_{nl}), dissipation (S_{dis}), bottom friction (S_{bf}) and wave breaking (S_{br}):

$$\mathrm{S} = S_{in} + S_{nl} + S_{dis} + S_{bf} + S_{br}$$

A detailed description is given by the WAMDI Group (1988), Komen et al. (1994), Günther et al. (1992), and Janssen (2008). The WAM Cycle 6 that is used for the Black Sea wave hindcast is an update of the former WAM Cycle 4. The basic physics and numerics are kept in that new release. The source function integration scheme made by Ardhuin et al. (2010) is incorporated. The wave model performance has been discussed in Stanev et al. (2014), Staneva at al. (2015; 2016a,b), Wahle et al. (2015), and in the recent Ocean State Reports #4 & #5 (von Schuckmann et al., 2020, 2021). Wave breaking has been taken into account. Time dependent depth and current fields are not used in this setup.

Data assimilation

In contrast to the previous MYP, the assimilation of measured satellite data have been taken into account. The required radar altimeter data for that purpose is available on the public server of AVISO (ftp-access.aviso.altimetry.fr) and includes, beside significant wave height, wind speed L2 data as well. The measured data will be assimilated into the wave model fields by the use of an sequential optimal interpolation scheme. The advantage of sequential methods in contrast to variational methods is the relative simplicity and the relatively small amount of required computer resources. The disadvantage is the fact that the significant wave height is not a dynamical quantity in the wave model, but only an output parameter derived from the spectrum. Therefore the procedure is split into two steps : first the SWH and wind speed data are used to construct analysed fields of SWH and wind speed by the OI and the second step consists of the reconstruction of the spectrum from the analysed fields. Since the wave model generates one-hourly output, the time of the satellite track can differ between 0 and 30 minutes from the nearest neighbour of the model grid points in time. The space error can be half of the mesh size of the spatial resolution of the model which is about 1.25 km. Quality control is included in the model so that unreasonable values are discarded automatically. Satellites cross the Black Sea once or twice a day in less than two minutes, so that very few measured values are available for assimilation into the wave and wind fields. Taking that into account and since the waves are propagating fast and have therefore a very small memory at that regional scale, we expect no significant influence of the assimilation on the wave model results. For the new MYP all radar altimeter measurements of the Jason-satellites that were available have been assimilated for the time periods that are covered by the three different Jason-satellites. Jason-1 data is assimilated for the first time period between 15/01/2002 and 21/06/2013, Jason-2 data between 22/06/2013 and 30/06/2019 and Jason-3 data between 01/07/2019 and 31/12/2021. Overlapping periods (04/07/2008 - 21/06/2013 and 12/02/2016 - 30/06/2019) are used for validation with independent satellite data

Forcing

The driving forces for the wave model are the U10 wind fields provided by the atmospheric reanalysis ERA-5 of the ECMWF (European Centre for Medium-Range Weather Forecasts). The U10 wind fields are disseminated through a corresponding ftp-server at a horizontal spatial resolution of 0.25°. The native spatial resolution of the ERA-5 wind fields is 0.28124 degrees which is about 31 km. The big advantage of the ERA-5 U10 wind fields as the driving force for the waves is the one-hourly availability in contrast to the 6-hourly ERA-Interim wind fields.

Boundary values are not considered as the Black Sea is a sem- enclosed area.

Wave growth

The growth of waves under extratropical wind storms and tropical cyclones has been the topic of several studies in the past two decades (Powell et al., 2003; Donelan et al., 2004; Zweers et al., 2010; Chen et al., 2013). Wave growth is controlled by the aerodynamic roughness of the surface, i.e., the drag that is felt by the wind. There is increasing evidence from theoretical (Makin, 2005), laboratory (Donelan et al., 2004;) and field studies (Powell et al., 2003; Holthuijsen et al., 2012; Donelan, 2018) that the roughness (and thus the drag) starts to level o
 or even drop (Powell et al., 2003) at very high wind speeds. Thus, how wave models parameterize wave growth under high winds becomes increasingly important as forecast systems, both coupled and uncoupled, move towards higher resolution (Li et al., 2021, Breivik et al, 2022)

To reduce possible underestimates of satellite radar altimeter measurements by the wave model, the parameterisation of the wave growth in the wind input source term has been adapted to the driving wind fields. The source term for the wind input is: The wave growth is controlled by the wind input term Sin. The form used in WAM Cycle 6 is based on the formulation presented as Eq. (19) by Ardhuin et al. (2010):

$$S_{\mathrm{in}} = \frac{\rho_{\mathrm{a}}\beta_{\max}}{\rho_{\mathrm{w}}\kappa^2} \mathrm{e}^Z Z^4 \left[\frac{u_*}{c}\right]^2 \max\left(\cos(\theta-\phi), 0\right)^p \sigma F(k,\theta).$$

Here, F(k;) [m3 rad1] is the wave variance density in wavenumber (k)-direction (ϑ) space, φ is the wind direction, β_{max} is a constant nondimensional growth parameter and

$$Z = \ln(k z_0) + \kappa/[\cos(\vartheta-\varphi)(u_*/c + z_\alpha)]$$

is an effective wave age with c the phase speed, the intrinsic circular frequency [rads-1] and z_0 a dimensionless wave age tuning parameter that shifts the growth curve. The directional spread is controlled by the power p, a tunable constant which is commonly (and here) set to 2. Higher powers give a more narrowly directed wind input.

It is important to note that Ardhuin et al. (2010) already introduced a cap on the surface roughness in the form

$z_0 = \min(\alpha_0 u^2/g, z_{0,\max})$

The growth rate, normalised by the angular frequency ω, derived from a parametrization by Janssen (1991) results from :

$\frac{\gamma}{\omega} = \varepsilon\beta x^2$

with ε the air-water density ratio, β the Miles parameter, and $x = \frac{u^*}{c}\max(\cos(\theta - \varphi), 0)$.

The Miles parameter β depends again on a constant called β_m with a default value of 1.2 after Janssen (1991). Here the β_{max} parameter has been tuned to $\beta_{max} = 1.8$ for the Black Sea to enable stronger wave growth.

In order to reduce possible underestimates of satellite radar altimeter measurements by the wave model, the parameterisation of the wave growth in the wind input source term has been adapted to the driving wind fields. The source term for the wind input is:

$S_{in} = \gamma F$ (wave growth * spectrum)

The growth rate, normalised by the angular frequency ω, derived from a parametrization by Janssen (1991) results from :

$\frac{\gamma}{\omega} = \varepsilon\beta x^2$

with ε the air water density ratio, β the Miles parameter, and $x = \frac{u^*}{c}\max(\cos(\theta - \varphi), 0)$.

The Miles parameter β depends again on a constant called β_m with a default value of 1.2 after Janssen (1991), but has been adapted to $\beta_m = 1.8$ for the Black Sea to enable stronger wave growth.

Partitioning method

Included in model outputs are characteristics describing individual wave components that make up a given sea-state. For example, a sea may consist simply of a single wind-sea component for which all wave energy is affected by the forcing wind, or multiple swell components, which have been remotely generated by distant storms. In WAM these components are determined using a two-stage process. Individual components are derived from the two-dimensional wave spectrum. This process effectively treats the wave spectrum as a topographic map from which individual peaks in wave energy can be identified to define the separate wave components.

The second part of the procedure follows an assumption that wind sea should be defined as only that part of the wave energy spectrum which is directly forced by the wind (this is an assumption, which is most regularly used by operational wave forecasters who wish to be able to reference the evolution of wind sea directly against evolution in the local wind conditions). Using this assumption, wave spectrum bins where wave speed is slower than the (co-directed) wind speed are associated with the wind sea component. The assignment of special energy to wind sea overrides any previous assignment of wave energy to the topographic components made in the first step.

III VALIDATION FRAMEWORK

The quality of the skill and temporal variability of the 73 years long reanalysis BLKSEA_MULTIYEAR_WAV_007_006, spanning the period 01 January 1950 to 31 December 2022 is assessed by comparing the simulated significant wave heights with measurements provided by a set of satellites, namely Jason-1, Jason-2, and Jason-3 covering reanalysis period from 2002 to 2021. For the comparison, we match significant wave heights from the satellites and BLKSEA_MULTIYEAR_WAV_007_006 in time and space. In addition, the CMEMS NRT dataset WAVE_GLO_PHY_SWH_L3_NRT_014_001 provided satellite data from Sentinel-3a/-3b, HaiYang-2b, Cryosat-2, CFOSat, and Saral/Altika. The CMEMS MY dataset WAVE_GLO_PHY_SWH_L3_MY_014_005 provided data from Cryosat-2, CFOSat, Saral/Altika, and Envisat. For the first 52 years between January 1950 and December 2001 there are no measurements available to compare with. As a precondition to enable these comparisons, the satellite data has to be correlated with the wave model data in space and time. The corresponding satellites need up to two minutes only to cross the Black Sea and the measurements recorded by the radar altimeter have been compared with the computed results of the nearest model output time. For each of the individual measurements with its unambiguous assignment to longitude and latitude, always the computed values of the nearest model grid point in space have been used to compare with.

Since the radar altimeter of the satellites measures wind speed and significant wave height, the only integrated wave parameter that can be used for validation is the significant wave height (SWH).

Although in-situ wave measurements from moored wave buoys are available from CMEMS In-Situ Thematic Assemble Centre (CMEMS INS TAC) (INSITU_BLK_PHYBGCWAV_DISCRETE_MYNRT_013_034) for the Black Sea, their locations are restricted to coastal areas of the southwestern basin. The corresponding water depths are mostly 17 m or 20 m and in the model domain, these positions are located at the land-sea boundary or only a few grids in the ocean. As the wave parameters are very sensitive to the water depth, the buoy positions in the model were slightly shifted (1-2 grids) in order to place them at a more realistic water depth. Time series at these grids have been used for validation.

Periods with obvious buoy measurement errors were detected and excluded from the validations. Further information about the Black Sea buoy data quality is currently not available but we established a collaboration with INS TAC to report measurement issues. This information will be used to, in turn, further improve the quality of the INS TAC data.

III.1 Quality control of the satellite data

Before making use of the satellites, the data need filtering to ensure physically plausible significant wave heights. Even though the data provided by AVISO (ftp-access.aviso.altimetry.fr) had been quality controlled, we found several cases that warranted further verification. Our quality control comprises manual and automatic filtering. At first, we screen the data to find obviously incorrect measurements, from which we derive criteria for automatic filtering. For instance, we remove all measurements, where the measured significant wave height equals 0. We also remove outliers that would possibly compromise our analysis. We define outliers as values farther away than 2 standard deviations from the linear slope-fit between measured and modelled data.

III.2 Statistical analysis

We present scatter plots that show measured against modelled significant wave heights for each of the satellites separately. We also consider the case, for which all the measurements are combined without distinguishing between satellites.

We illustrate overplotting (as there are thousands pairs of measured and modelled data) by estimating the bi-variate probability density by evaluating a 2d-Gaussian kernel on a square grid in the variable space (Venables and Ripley, 2002).

Furthermore, the plots include summary statistics, such as the mean value and standard deviation, and statistics that describe the skill of WAM to simulate the significant wave heights for the time period January 2002 to December 2021.

The skill scores used are Pearson's product-moment correlation coefficient (Corr), the root mean squared difference (RMSD), the bias, the scatter index (SI) (e.g. Chawla et al., 2013), and the reduction of variance (RV). The scores read as follows, where o and m stand for observed and modelled data. An overbar over a variable denotes the temporal average value derived from the sample of length n.

$$Correlation = \frac{\frac{1}{n-1}\sum_{i=1}^{n}(o_i - \bar{o})(m_i - \bar{m})}{\sqrt{\frac{1}{n-1}\sum_{i=1}^{n}(o_i - \bar{o})^2}\sqrt{\frac{1}{n-1}\sum_{i=1}^{n}(m_i - \bar{m})^2}}$$

$$RMSD \sqrt{\frac{1}{n}\sum_{i=1}^{n}(m_i - o_i)^2}$$

$$BIAS = \frac{1}{n}\sum_{i=1}^{n}(m_i - o_i)$$

$$SI = \frac{\sqrt{\frac{1}{n-1}\sum_{i=1}^{n}(m_i - o_i - BIAS)^2}}{\sigma}$$

$$RV = 1 - \frac{\sum_{i=1}^{n}(m_i - o_i)^2}{\sum_{i=1}^{n}(o_i - \bar{o})^2}$$

One of the general assumptions for the correlation coefficient is that variables follow a normal distribution, which is not the case for the significant wave height. It might be advisable to use another measure to gauge the monotonic relation between modelled and observed significant wave heights, such as the rank correlation. However, we use Pearson's correlation coefficient as it is a quasi-standard for evaluating numerical models. Note that the skill metric RV is an adaptation of the Brier Skill Score and gauges the error variance (assuming a zero-mean error) against the variance of observations. RV is bound by $-\infty$ and one. While the latter stands for perfect model skill, negative values would indicate no skill at all. As the error variance, here expressed as the sum of squared errors, can be decomposed into components related to the standard deviations and the correlation coefficient, RV not only depends on the magnitude of errors but also on the capability of WAM to simulate the temporal variability of the wave fields (see Murphy and Ebstein, 1989).

The scatter plots also show the least-squares linear fit without including any intercept between measurements and modelling results. Ideally, such a fit would be close to the straight line dividing the scatter plot at an angle of 45°, which is included as a reference.

Last, we also show pairs of quantiles of the measured and modelled significant wave heights. The quantiles are estimated from the empirical cumulative density function at specific percentiles. The highest quantile shown corresponds to the sampled maximum value, which translates to the 100th percentile of the empirical distribution.

Furthermore, we also provide the skill scores on the annual and seasonal scale as time series.

III.3 Time series analysis

The length of the combined satellite measurements allows further assessing the quality of the dataset through computing time series of statistical properties, which are derived on shorter time scales. We assume that already monthly intervals would contain enough information to represent the Black Sea properly, but increasing time scales further improves the informational content. Short time scales are potentially affected by the data availability of the satellites: The duration of one satellite passing over the Black Sea lasts for less than two minutes only. Fly-overs happen once to twice daily. Consequently, very short statistics, e.g. on the daily scale, would not represent the Black Sea waves adequately. Therefore, we have chosen to use the annual scale in the following.

We compute time series of specific quantiles, mean, minimum, and maximum values of measured significant wave heights for each year in the measurement period of the satellites. We apply this procedure to the corresponding simulated significant wave heights from WAM for a comparison. The quantiles have been selected to represent the whole distribution of significant wave heights with a focus on the upper quantiles. Similar to the scatter plots we provide the correlation, bias, and RMSD, but also include the relative error, which reads

$$RErr = \frac{\frac{1}{n}\sum_{i=1}^{n}(m_i - o_i)}{\sigma}$$

Note that this method heavily depends on the location and time of the satellite tracks and cycles. Likely, our approach does not catch all notable wave events. However, by using a relatively long interval to aggregate statistics, we can assume that our statistics are robust and, as a time series, can represent the wave climate of the Black Sea.

IV VALIDATION RESULTS

IV.1 Statistical analysis

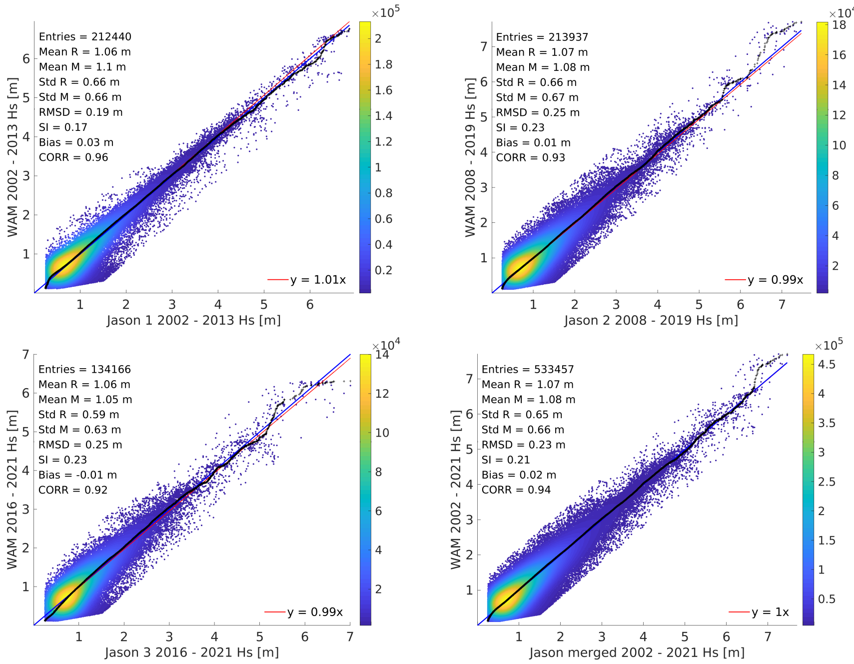

Figure 3: Scatter plots showing satellite measurements versus modelled significant wave heights for the periods 2002-2013 (Jason-1), 2008-2019 (Jason-2), 2016-2021 (Jason-3), and 2002-2021 (all satellites merged). Also shown are the estimated bivariate probability density (coloured area), the linear slope-fit regression of modelled and observed wave heights (red line), specific quantiles taken from the empirical cumulative density function (black line), and the diagonal (blue line). Furthermore, summary statistics and skill scores are included. R: reference (satellite) data, M: model data.

Figure 3 depicts the scatter plots for the comparison between modelled significant wave heights and the satellites (Jason-1, Jason-2, Jason-3 and the combination thereof). In general, all the computed and measured mean values of SWH are located between 1.0 and 1.1 m. The bias is nearly zero for all the merged satellite values, although the values for Jason-1 and Jason-2 show a very slight overestimation of the wave heights in WAM. The calculated biases of WAM for the different satellites confirm the good agreement between measurements and model results being in the range of -0.01 m (Jason-3) to 0.03 m (Jason-1). Noteworthy is that the full range of SWH shows almost no deviations from the 45°-line. The RMSD, on which the bias has a strong influence and which represents the magnitude of model errors, varies from 0.19 m (Jason-1) to 0.25 m (Jason-2 and -3). Another source of the deviations lies in the difference of the simulated and modelled variability, here given as the standard deviations. The differences range from about 0 cm (Jason-1) to 4 cm (Jason-3). Note that measurement errors and noise that our initial quality control has not filtered out can also impact the RMSD and the standard deviation of the measurements, thus potentially degrading the model skill. Additionally, the wind fields also influence the model variability and skill as they force the wind-wave model WAM. The forcing fields reflect real atmospheric winds only to a certain extent regarding magnitude and variability as they come from the spatially coarse (0.25x0.25°) one-hourly ERA-5 reanalysis (see also Section IV.5).

However, contrary to these deficiencies, the correlation, as a measure of how well the wave heights of WAM and of the satellites are positively linearly related, is in the range of 0.92 (Jason-3) to 0.96 (Jason-1) showing a strong linear relationship. Furthermore, the scatter index SI support the skillfulness of WAM as they are relatively low with values between 0.17 for Jason-1 to 0.26 for Jason-2 and -3. The scatter index benefits from the high correlations as the correlation counteracts the influence of the bias and the RMSD in SI. Note that in comparison with skill assessments from short-term wave analyses and forecasts (see QUID for BLKSEA_ANALYSISFORECAST_WAV_007_003 for instance), the overall skill of the long reanalysis product is slightly lower due to the long period examined, in which systematic biases, measurement errors and noise can accumulate.

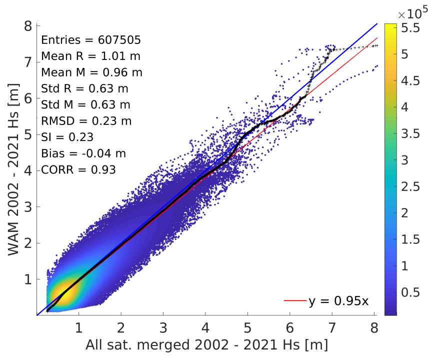

Figure 4: Scatter plot showing satellite measurements versus modelled significant wave heights for the period 2002-2021 using the non-assimilated satellites Sentinel-3a/-3b (NRT), HaiYang-2b (NRT), Cryosat-2 (NRT+MY), CFOSat (NRT+MY), Saral/Altika (NRT+MY), and Envisat (MY) (all satellites were merged).

The good model skills in Figure 3 could be related to the fact that the underlying satellite data is assimilated into the model system. To confirm the results, another scatter plot was prepared (Figure 4), which compares the model data with non-assimilated satellite altimeter data, namely Sentinel-3a/-3b, Cryosat-2, CFOSat, Saral/Altika, and Envisat. It is highlighted that the model skill is almost the same compared to the skill including assimilated satellite data. The RMSD is of the same magnitude (23 cm), the SI is 2% worse, the bias is 6 cm less (-4 cm), and the correlation is 0.01 lower. As a result of the negative bias, the slope is 0.05 lower.

Figure 5 includes time series of different statistical parameters for the complete validation period between 2002 and 2021. On that annual scale, the metrics show that the skill that can be seen in all of the statistical parameters is versatile for the individual satellites. The general metrics behaviour can be described as follows. During the assimilation periods of the individual satellites, the metrics are relatively constant (RMSD: 18 cm, bias: 5 cm, correlation: 0.97, SI: 0.17, and RV: 0.92), whereas the not assimilated periods show slightly decreased quality of statistics. For example, the RMSD increases to ~30 cm, the bias to -5 cm, the correlation to 0.88, the SI to 0.30, and the RV to 0.75. Nevertheless, even those metrics can still be considered as good model performance.

Overall, the skill scores depend on the number of collocated measurements to some extent. It is obvious that with decreasing number of observations, the values for the statistical parameters as RMSD, bias, and scatter index go up, while those for the reduction of variance and the correlation go down.

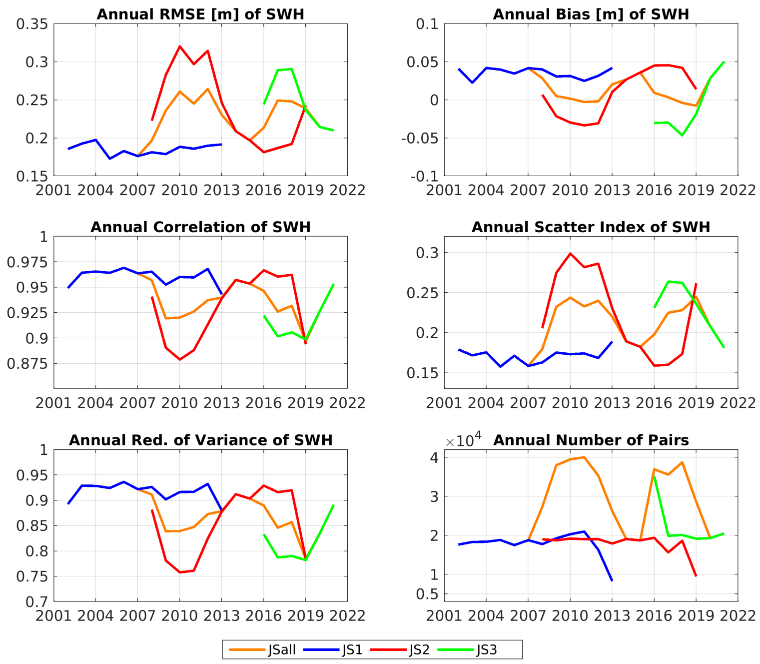

Figure 5: Yearly values of significant wave height metrics for the Black Sea derived from individual and combined satellite measurements.

Figure 6 shows the time series of the annual 99th and 99.9th percentiles for the significant wave heights generated by the wave model, those recorded by the radar altimeters of the Jason satellites and the differences in the significant wave heights between both. The time series of 99th and 99.9th percentiles show a constant variability around 3.5 and 5 m for both the model and satellite data. Also among the single satellites, the differences are rather low and the large discrepancies occur around 2013 when the and of the Jason-1 life time was reached.

The 99th and 99.9th percentiles of the SWH differences between the model and the satellites reveal a similar behaviour that the metrics in Figure 5; when the satellite data is assimilated, the percentiles decrease. When assimilated, only 1% of the differences are higher than 40 cm and 0.1% higher than 60 cm. If assimilated, the values increase to 70 and 100 cm, respectively.

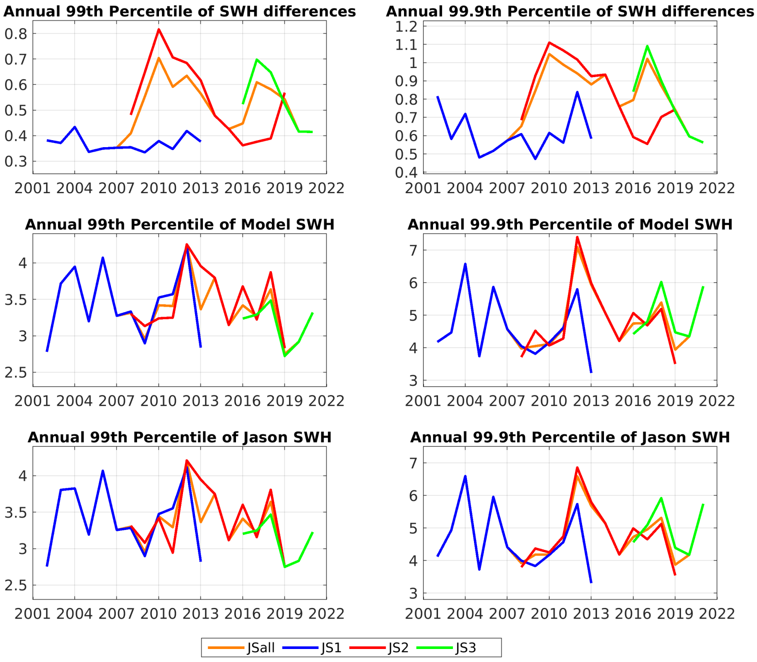

Figure 6: Annual percentiles for the differences of the significant wave height, the model wave height and the wave height recorded by the radar altimeter of the satellites (on the left: 99th percentiles, on the right: 99.9th percentiles).

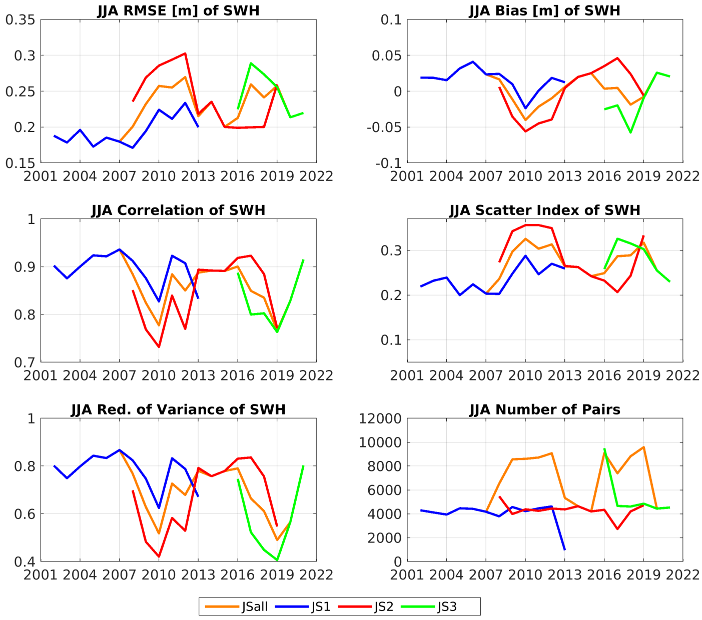

Figure 7: Annual values of summer (JJA)-significant wave height metrics for the Black Sea derived from individual and combined satellite measurements.

Seasonal metrics as shown in Figure 7 and 8 reflect the temporal evolution of the annual skill metrics. Yet, there are some notable differences visible. First, the skill as measured by the RMSD and bias seems better in the summer seasons (JJA) than in the winter seasons (DJF), where the RMSD (bias) ranges from about 0.17 to 0.30 m (-0.06 to 0.05 m) in JJA, and from 0.16 to 0.35 m (-0.07 to 0.07 m) in DJF. Considering that winds are calmer over summer, wind-waves are consequently smaller in JJA, which reduces the error measurements that base on absolute significant wave heights. However, the correlation and the reduction of variance skill scores point to the opposite. In DJF, they range from about 0.74 to 0.94 (0.40 to 0.86) for the correlation (reduction of variance). In JJA, the correlation ranges from 0.86 to 0.98, the reduction of variance from 0.70 to 0.97. Both metrics indicate that the skill of WAM to simulate the wave fields during summer is decreased compared to the DJF season. Similarly, the SI shows better values in winter (0.10 to 0.26) than in summer (0.20 to 0.34). This different behaviour of the statistics in summer and winter is explained by the mean wave height, which is lower in summer. In turn, lower mean values worsen the metrics correlation, SI, and RV if similar relative differences of model-satellite pairs are assumed as they include temporal means (see Section III.2).

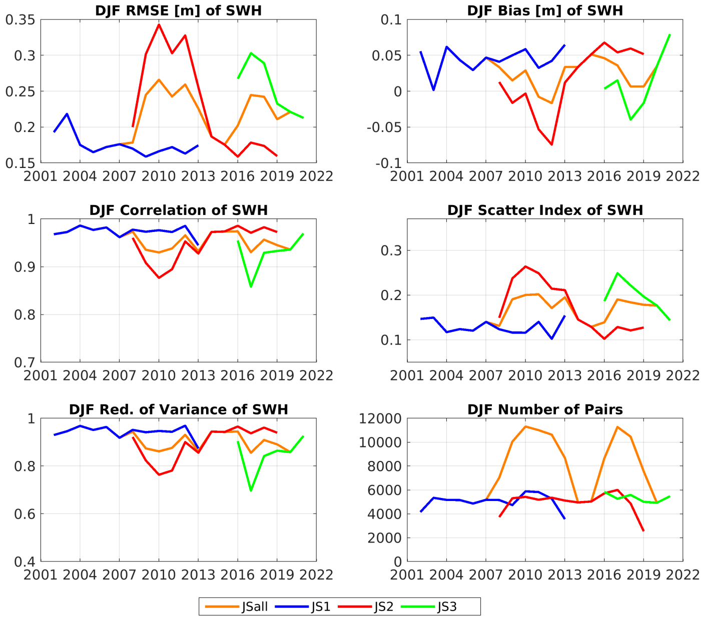

Figure 8: Annual values of winter (DJF)-significant wave height metrics for the Black Sea derived from individual and combined satellite measurements.

IV.2 Error maps

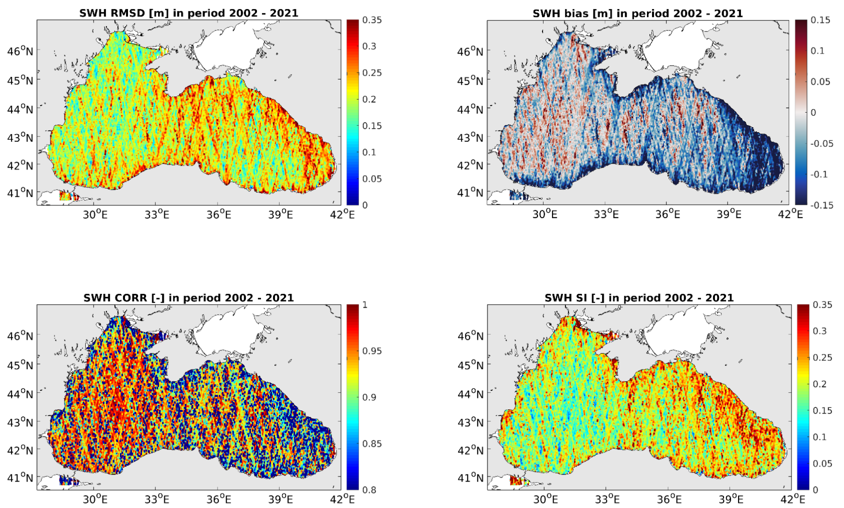

Figure 9: Spatially varying metrics of significant wave height obtained from the same non-assimilated satellite data as presented in Figure 4. The metrics are obtained by gridding the satellite data onto the model grid and performing the assessment grid-wise. RMSD: upper left, bias: upper right, correlation: lower left, and scatter index: lower right. The maps are smoothed with a box filter.

Despite knowing the overall metrcis and their dependence on time, it is also important to determine subregions of the domain with unusual high or low model skills. A first attempt is presented in Figure 9 showing the modekl skills obtained from the non-assimiated satellite data grid-wise. The results reveal that southern, eastern, and north-eastern coasts have decreased models skills, e.g. the bias is negative, whereas the inner basins and the western/north-western coasts reveal a very good model skill. The single metrics vary approximately as follows: the RMSD ranges between 15 and 30 cm, the bias between -15 and 5 cm, the correlation between 0.80 and 0.97 and the scatter index between 0.13 and 0.30.

IV.3 Buoy validations

The time period from May 2020 to December 2021 is (partly) covered by the time series of eleven wave buoys. Their locations and names are shown in Figure 10. The WAVEBXX and WD3044 buoys are mounted at a water depth of 17 m and the SPOTXXXX buoys at 20 m. They provide the variables significant wave height, maximum wave height, wave mean direction, wave peak direction, wave T_{M02} period, and wave peak period (however, not consistent among all buoys). For a visual demonstration of the model performance, one buoy (WAVEB03) has been chosen and its results are presented in the following (Figure 11-17) as time series. The available buoy time series cover the 6-month period from July 2021 until December 2021.

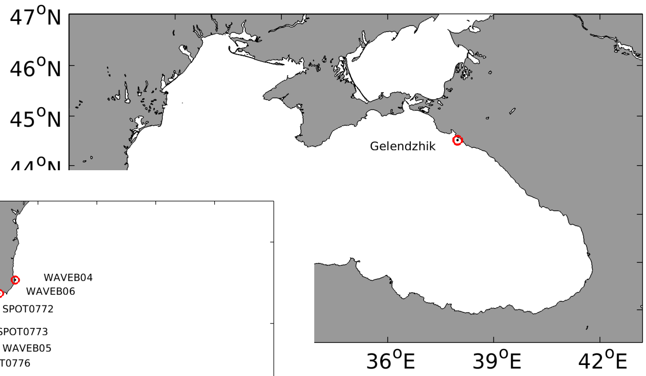

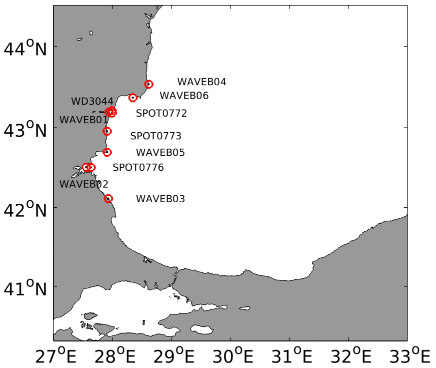

In the case of significant wave height, the model performs well over the whole 6 months (Figure 11). The performance is good in both, the SWH magnitude and the timing. The corresponding scatter plot (Figure 12) shows a relatively constant overestimation of the modelled SWH of 12 cm over whole range of wave heigths. It is assumed that the vicinity to the coast and probable uncertainties in the model bathymetry negatively influence such a comparisons. Despite that, the overall metrics are still good with values of bias = 12 cm, RMSD = 20 cm, SI = 0.21, and CORR = 0.96.

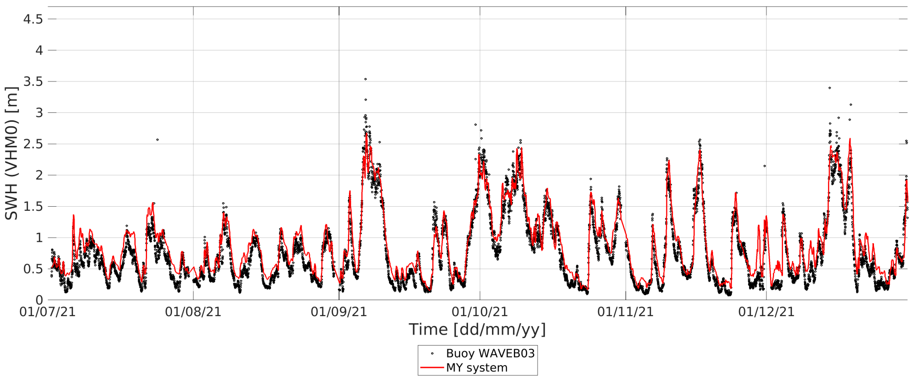

Figure 11: Significant wave height (VHM0) of the buoy WAVEB03 (all available data).

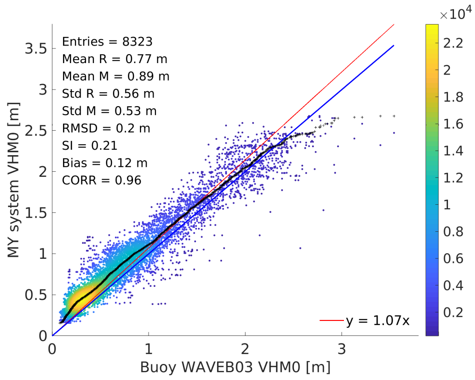

Figure 12: Scatter plot of significant wave height (VHM0) of the WAVEB03 buoy vs. model for the period shown in Figure 11. See Figure 3 for a detailed description of the scatter plot.

The availability of in-situ observations made it possible to perform validations not only for the SWH but also for other wave variables. The wave T_{M02} period (Figure 13) shows a similar behaviour then SWH. The timing is very good over the whole period but a slight overall underestimation is present. However, this underestimation is mostly less than 1 s (overall bias is -0.32 s), thus we can consider that the validations show good agreement against the observations for the T_{M02} period. It has to be noted that higher periods (higher than ~5 s) stronger deviate from the measurements (underestimated) than shorter periods.

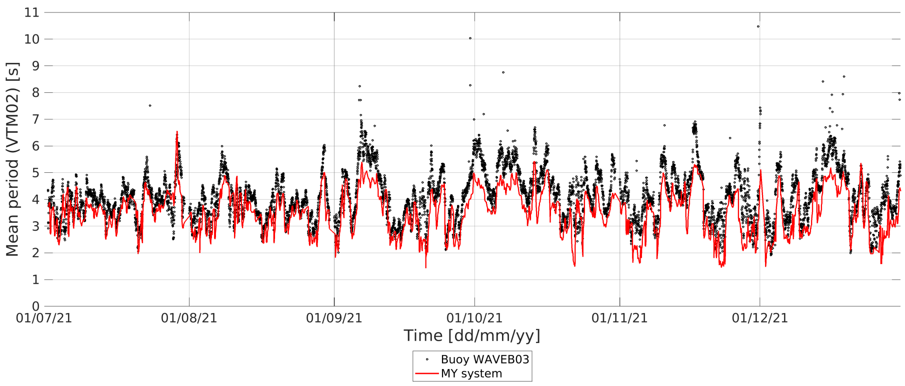

Figure 13: Wave T_{M02} period (VTM02) of the buoy WAVEB03 (all available data).

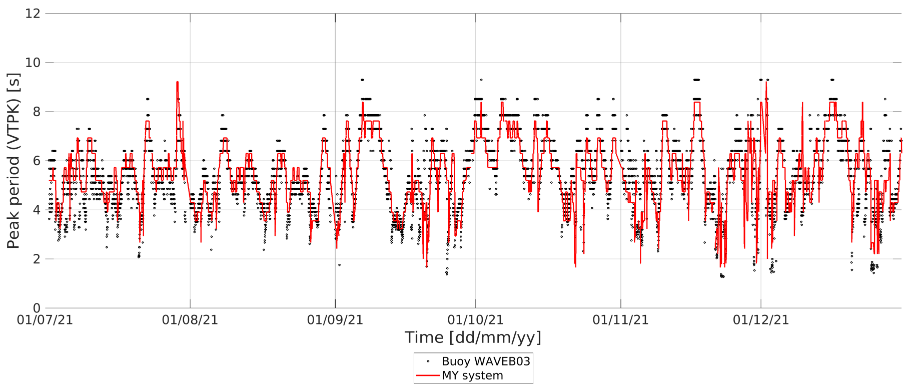

Figure 14: Wave peak period (VTPK) of the buoy WAVEB03 (all available data).

In contrast, the peak period is less underestimated (Figure 14) and the model performance of this variable is even better (overall bias is 0.02 s).

The simulated wave mean direction matches well with the in-situ data (Figure 15). Also, the short-term variations are well captured by the model. This good performance could be related to both the improved spatial resolution and the updated source terms. The performance of the wave peak direction (Figure 16) is comparable to the wave mean direction.

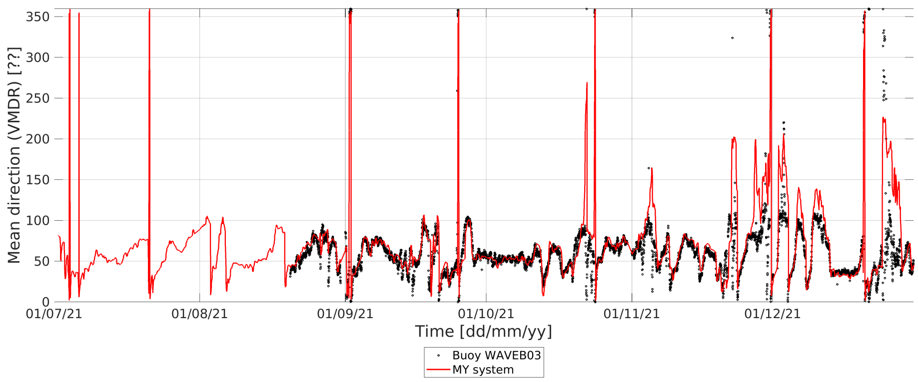

Figure 15: Wave mean direction (VMDR) of the buoy WAVEB03 (all available data). Vertical red lines appear due to the change from 359 to 0°.

The buoy WAVEB03 does not provide maximum wave height data. Thus, the results of the buoy WAVEB01 are used instead (Figure 17) to demonstrate the model performance of the wave variable VZMX. The buoy WAVEB01 is located further north in the Gulf of Varna (see Figure 10).

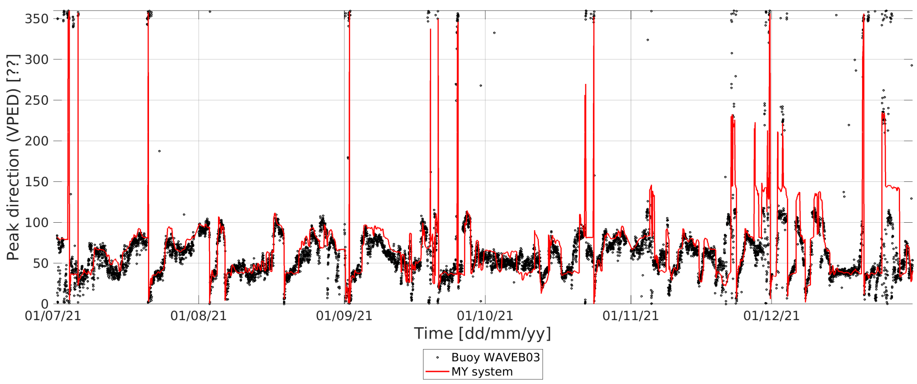

Figure 16: Wave peak direction (VPED) of the buoy WAVEB03 (all available data). Vertical red lines appear due to the change from 359 to 0°.

Compared to the significant wave height, the timing of Hmax is slightly worse. In addition, the maximum wave height simulation is also worse in terms of amplitudes, which could be due to the different type/location of the buoy. However, the overall model performance can still be considered as good.

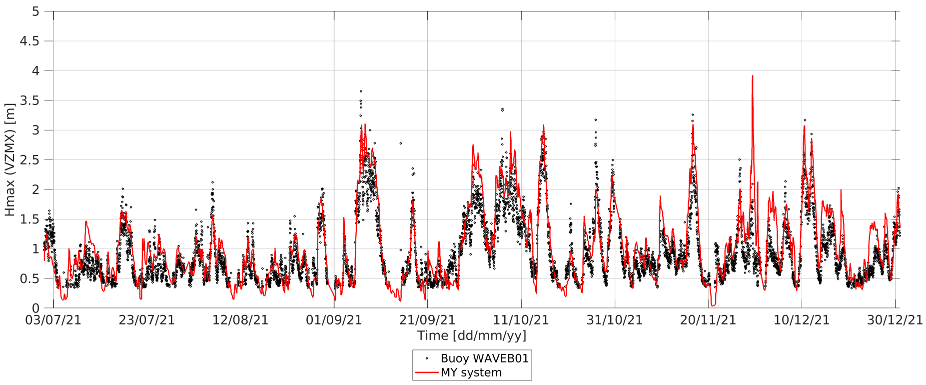

Figure 17: Maximum wave height (VZMX) of the buoy WAVEB01 (all available data). Hmax is not available for WAVEB03; instead WAVEB01 is shown.

When taking into account all buoys and all available buoy data for the considered period, the bias and RMSD of significant weight are 12 and 21 cm, respectively (Table 2). As buoy data is not assimilated into the model, these metrics are good values and also other variables like VTM02, VTPK, VMDR, and VPED show relatively slight deviations from the measurements. Only VZMX shows lower performance.

Although the model-buoy comparisons reveal good model skills, it is noteworthy that the buoy data contain periods with possibly reduced data quality. Especially, the wave directions could be influenced by unprecise calibrations. As noted earlier, we established a collaboration with INS TAC to report measurement issues.

*Table 2: Overall metrics for the MY BS-waves system using all **buoys**.*

Period: May 2020 to December 2021		
Variable	Bias [cm]	RMSD [cm]
VHM0	10 cm	19 cm
VZMX	11 cm	37 cm
VTM02	-0.3 s	0.9 s
VTPK	0.0 s	1.3 s
VMDR	-9°	56°
VPED	-15°	61°

IV.4 Comparison at location Pasha Dere – Storm representation

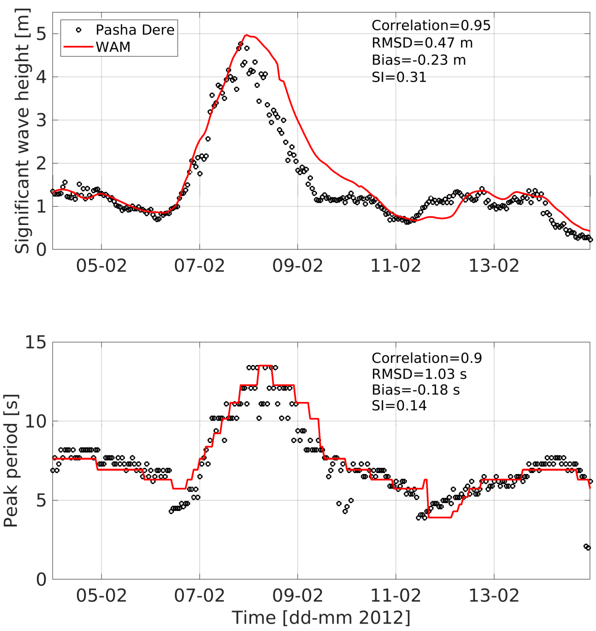

Figure 18: Significant wave height and peak period from WAM and from the ADCP station Pasha Dere in the period 04-15 February 2012.

For the period between 04 February 2012 to 15 February 2012, ADCP data at the location Pasha Dere (located at 28.03 °E, 43.08 °N) in the western part of the Black Sea near the Bulgarian coast was available. This period covers a storm event occurring between 07 and 09 February 2012. The comparison with WAM for the significant wave height and peak period is shown in Figure 18. The measured and modelled time series of the significant wave height and peak period show very good agreement. Although the skill scores for the significant wave height are not perfect (bias: 24 cm, RMSD: 47 cm, correlation: 0.95, and SI: 0.31), the shape of the curve is often well captured. The corresponding values for the peak period, which depends sensitively on the resolution of the model frequency, are also very good with a bias of 0.2 s, a RMSD of about one second, a correlation of 0.90, and a SI of 0.14. Additionally, the storm peak was simulated quite accurately in terms of amplitude. However, the SWH decrease is slightly delayed, which is the reason for the decreased metrics. Nevertheless, this comparison illustrates nicely the capacity of the wave model to represent the arrival of a captured storm.

IV.5 Time series analysis

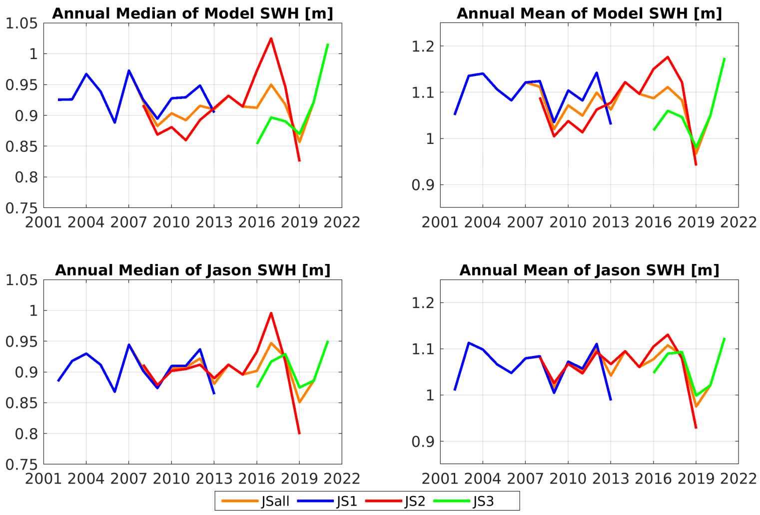

Figure 19: Time series of annual median and annual mean of the significant wave height along the satellite tracks shown for model (upper row) and satellite data (lower row).

Time series of wave statistics derived from satellites and WAM gives the chance to examine the temporal variability of specific parts of the wave height distribution and allow further assessing the skill of WAM. Figure 19 includes the time series of the annual median and the annual mean of the significant wave height for the model in the upper row and the satellites in the lower row. While the annual median for the WAM wave heights shows values between 0.82 and 1.02 m, the annual mean is slightly higher with values between 0.95 and 1.17 m. For the annual median and the annual mean of the satellite measurements, the same is valid. Here the values for the median range between 0.80 and 1.00 m whereas those for the annual mean range between 0.92 and 1.13 m. An interesting feature here is the significant increase and following decrease of the Jason-2 wave height at the end of its lifetime in contrast to the Jason-3 data that starts in 2016 and generates much smaller values.

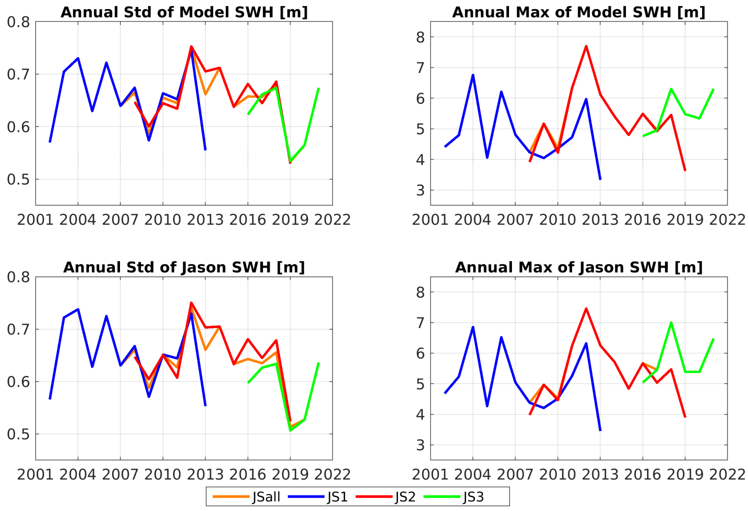

Figure 20: Time series of annual standard deviation and annual maximum of the significant wave height along the satellite tracks shown for model (upper row) and satellite data (lower row).

Furthermore, Figure 20 gives an overview of the annual development of the standard deviation and the maximum of the significant wave heights for WAM in the upper row and for the satellites in the lower row. The curves for both variables are very similar when comparing the model and satellite data. For the standard deviation, values range between 0.53 and 0.75 m and for the annual maximum between 3.4 and 7.7 m.

As shown in the uppermost row of Figure 21, the mean annual wave heights range from around 1.00 to 1.15 m without an obvious trend from 2002 to 2021 in WAM with similar and sometimes slightly lower values in the satellite measurements. In 2019, the lowest annual mean occurred, whereas 2021 has the highest annual mean. The annual maximum significant wave heights derived from satellite measurements and WAM show a correlation of about 0.97, which demonstrates that WAM can simulate the temporal variability of maximum wave heights well.

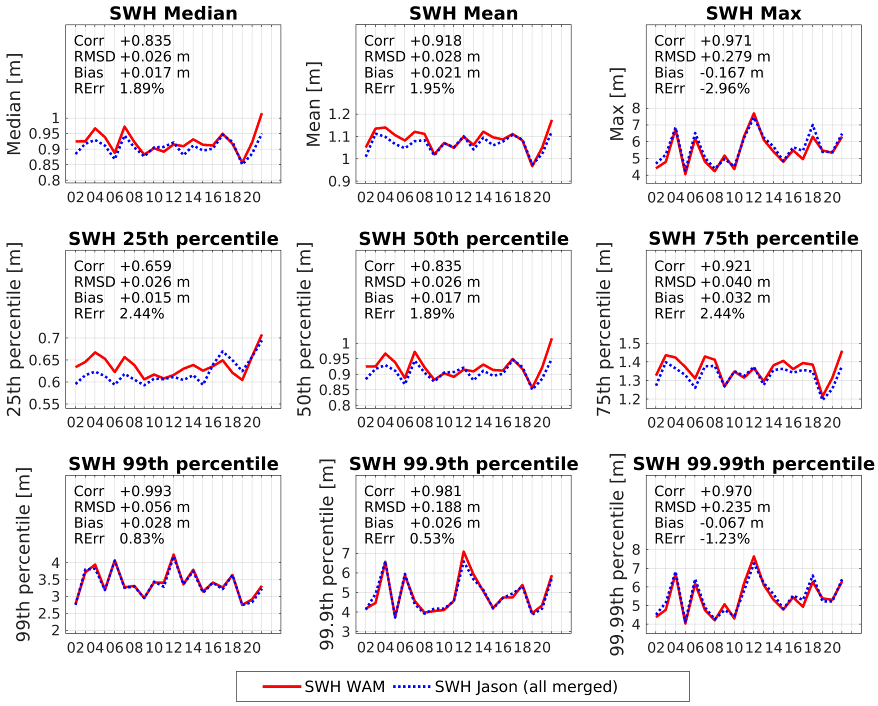

Figure 21: Time series of annual median, mean, and maximum of the significant wave heights, as well as time series of specific annual quantiles of significant wave heights derived from all Jason satellite measurements and from WAM.

WAM slightly underestimates the maximum wave height resulting in a bias of -17 cm (corresponding to a relative error of 2.44% in Figure 21, the upper panel on the right). There are three years 2016 and 2018, for which the maximum significant wave heights are a bit underestimated. However, 2012 reveals the highest annual maximum significant wave heights, which are also simulated quite well.

Making use of the annual time scale that provides enough samples to examine quantiles even higher than the 99th percentile and helps to understand the peak values in 2004 and 2016 to transitioning from the lower parts of the distribution to the uppermost part. The row in the middle and the lowermost row of Figure 21 show the percentiles of the significant wave height, starting with the 25th, the 50th and the 75th percentile in the middle row and including the 99th, the 99.9th and the 99.99th in the lowermost row. The annual quantiles of significant wave heights from the 25th to the 99.99th percentiles representing almost three-quarters of the distribution show a temporal behaviour very similar to that of the annual mean significant wave height. The correlation between wave model results and satellite data increases with higher percentiles with a maximum value of 0.99 for the 99th percentile. That demonstrates very good skill in catching the variability of high wave heights in the Black Sea. In contrast, the lower 25th, 50th, and 75th percentiles how lower correlations and are underestimated. The skill of WAM thus increases with higher percentiles, which possibly relates to parametrisations within WAM that slightly degrade the skill for smaller wave heights in favour of larger waves (von Schukmann et al., 2020).

While the annual 99th percentile shows a variability evenly distributed over the whole period with a very good agreement in the time series behaviour, the 99.9th and 99.99th percentiles in WAM become dominated by the peak in 2012. These very high percentiles represent only a very small number of observations attributable to single events that do not affect lower quantiles of the distribution markedly.

Several factors might influence the assessment of significant wave heights. First, the wind-wave model WAM, for which simulated wave heights depend on the wind forcing to a large extent, needs wind fields that include high wind speeds at the right time and space to model wave heights in agreement with satellite observations. Here, the used wind fields are taken from the ERA5 reanalysis, which provides data in a one-hourly resolution. It seems that this temporal resolution of the wind forcing is necessary to simulate the upper percentiles correctly.

Finally, the satellites measure wave heights along tracks in a very fine temporal and spatial resolution that is much more detailed than the simulated wave fields of WAM. In our analysis, we match satellite measurements with their closest match in WAM introducing a sampling error that affects all parts of the wave distribution in our analysis. An even stronger effect could have the relatively coarse lateral resolution of the ERA5 wind fields.

IV.6 Along-track validations

From all storms that were identified during 2002-2021, considering a threshold of 3.5 m significant wave height, Figures 22, 23, and 24 show examples of three storm situations. The first one in Figure 23 describes the conditions on the 8th of February 2012 at 14:00 UTC in the Black Sea highlighting the distribution of significant wave height and wave direction overlaid by a descending Jason-1 track that corresponds in time. The satellite crosses the south-western basin of the Black Sea with SWH up to 6 m. The along-track comparison on the right of Figure 22 is supporting the very good agreement between the wave model results and the satellite data.

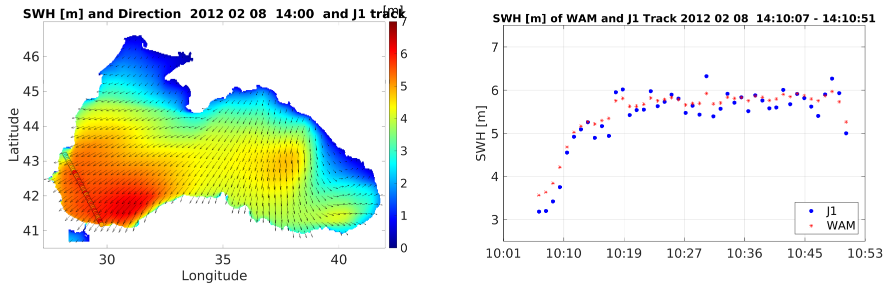

Figure 22: Distribution of significant wave height of WAM with overlaid Jason-1 satellite track (left) on 08/02/2012 14:00 UTC and time series of measured and computed significant wave height along the satellite track (right). Solid black circles: locations of the tracks. The x-axis represents time [hh:mm] of the day and hour given in the title. Arrows denote the satellite flight direction

The second example deals with an ascending Jason-2 satellite path that crosses a storm area in the eastern basin of the Black Sea. The corresponding distribution of wave height and direction is given in Figure 22 (left). As in the previous example, the agreement between measurements and wave model results is nearly perfect as demonstrated in the along-track time series on the right of Figure 22. The wave heights in the maximum are around 5.5 m.

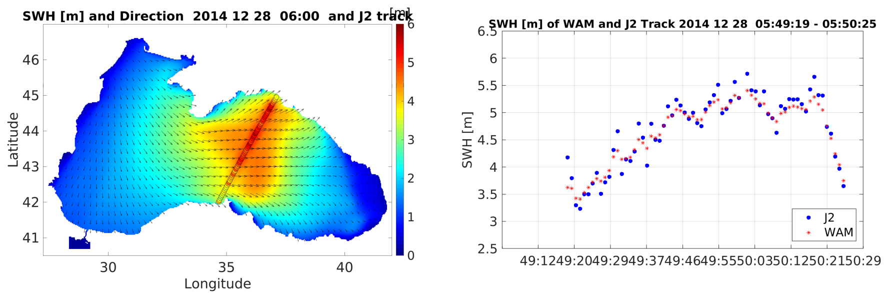

Figure 23: Distribution of significant wave height of WAM with overlaid Jason-2 satellite track (left) on 03 December 2016 06:00 UTC and time series of measured and computed significant wave height along the satellite track (right). Solid black circles: locations of the tracks. The x-axis represents time [hh:mm] of the day and hour given in the title. Arrows denote the satellite flight direction

The third example shows a descending Jason-3 track passing a storm area in the eastern basin. This example is very similar to the previous one. The wave heights in the maximum are around 6 m.

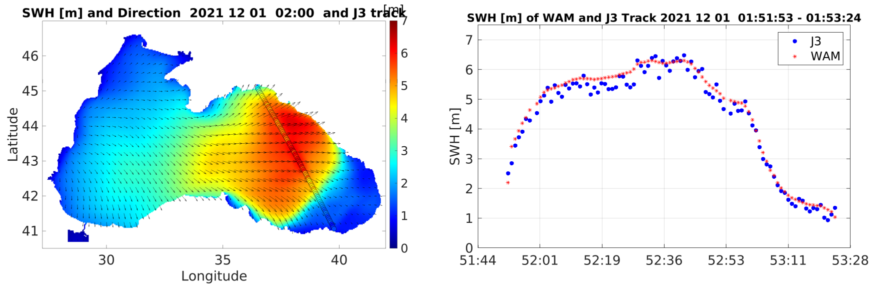

Figure 24: Distribution of significant wave height of WAM with overlaid Jason-3 satellite track (left) on 03 December 2016 06:00 UTC and time series of measured and computed significant wave height along the satellite track (right). Solid black circles: locations of the tracks. The x-axis represents time [hh:mm] of the day and hour given in the title. Arrows denote the satellite flight direction.

IV.7 Wind validations

The wind forcing is the most important forcing of the wave model. Thus, it is of utmost importance to determine its quality. As in-situ measurements of wind (e.g. from buoys) are lacking, the validation is restricted to satellite-obtained wind speed. This quantity is also contained in the AVISO L2 satellite data. The assessment approach is the same as for the SWH (see Figure 3). The comparisons are shown separately for each available satellite (Figure 25) as well as for all satellite data merged (Figure 25, lower left panel). The wind forcing slightly overestimates the moderate winds whereas the low and high winds are represented quite well (see the qq-plot and the diagonal). Very high winds (>~12 m/s) tend to be too low in the forcing. The data of all satellites are quite close to the y-x line and the qq-plots show relatively low deviations from the diagonal resulting in biases of 0.06 to 0.26 m/s (subfigures of Figure 25). The RMSD ranges from 1.43 to 1.44 m/s with a SI of 0.23 to 0.24. The CORR is also relatively constant with values of 0.85 to 0.86. For all satellites together, the respective values are: bias = 0.19 m/s, RMSD = 1.44 m/s, SI = 0.24, and CORR = 0.86. In summary, the quality of the wind forcing can be considered as good. However, the wind direction is not taken into account and is still an unverified error source.

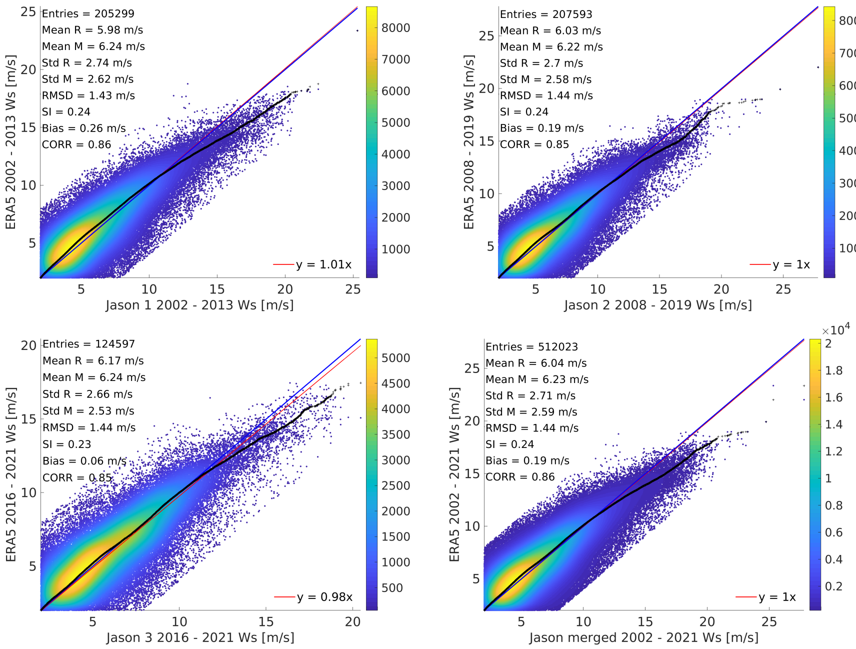

Figure 25: Scatter plots showing satellite measurements versus wind speeds (ERA5) for the periods 2002-2013 (Jason-1), 2008-2019 (Jason-2), 2016-2021 (Jason-3), and 2002-2021 (all satellites merged). Also shown are the estimated bivariate probability density (coloured area), the linear slope-fit regression of modelled and observed wave heights (red line), specific quantiles taken from the empirical cumulative density function (black line), and the diagonal (blue line). Furthermore, summary statistics and skill scores are included. R: reference (satellite) data, M: model data.

V ANNEXES

V.1 Mean state

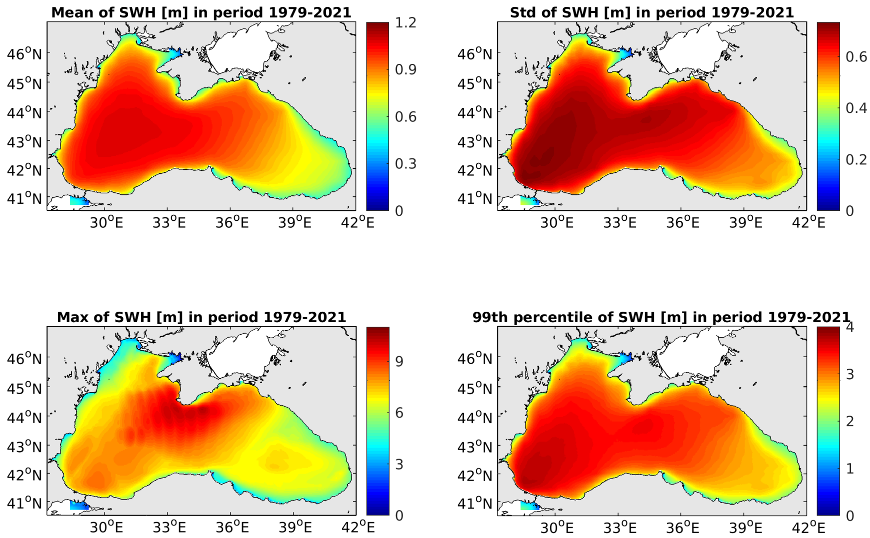

Figure 26: Average (upper left), standard deviation (upper right), maximum (lower left), and 99th percentile (lower right) of significant wave height in WAM calculated over the period 1979-2021.

Figure 26 shows the mean, the standard deviation and the maximum of the significant wave height calculated over the period 1979-2021. The highest mean significant wave heights are found in the southwest with significant wave heights of up to 1.1 m on average. In this region, the fetch from the dominating directions is long (see Figure 27). The waves become smaller in the eastern parts of the Black Sea. Here, the fetch from the western directions is not apparent, as we do not find waves as high as in the western part. The standard deviation ranges between 0.4 m in coastal areas to 0.7 m in the western part of the Black Sea. The standard deviation is high on average where the mean significant wave heights are large. Regarding the maximum significant wave height, we see that the highest waves are found in the northern part of the central body of the Black Sea with values up to 9.5 m. Further local maxima can be detected in the south-west and in a small area in the south-east. The spatial distribution of the maximum wave height reflects single strong storm events causing high waves. The distribution of the 99th percentile of the significant wave height proves that most of the wave heights are below ~4 m with a maximum in the southwest of the Black Sea.

Beside the significant wave height, it is worthwhile to have a look on the distribution of the mean wave directions in the Black Sea. Those are shown in Figure 27 in the atmospheric convention “coming from”.

The dominant wave direction in the western part is to the west/south-west. In the eastern part, the waves on average go to the east/south-east. In the southern central body of the Black Sea, the waves propagate on average to the south, whereas in the northern parts around the Crimean Peninsula the directions changes. The size of these areas with different directions varies. In general, the waves propagates in direction to the coasts of the Black Sea.

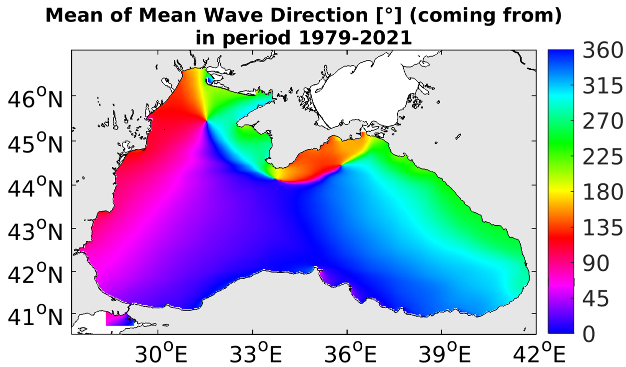

Figure 27: Average of the annual mean wave direction in WAM calculated over the period 1979-2021 shown in the "coming from" convention.

V.2 Histograms

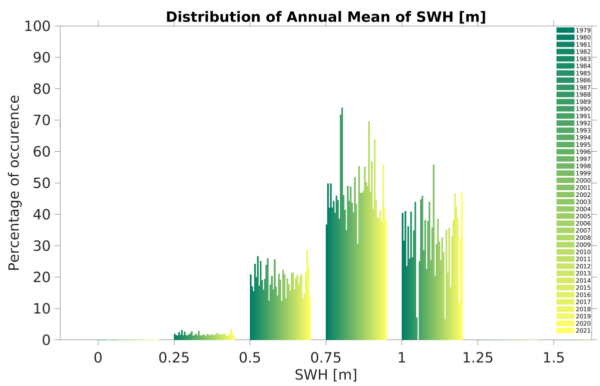

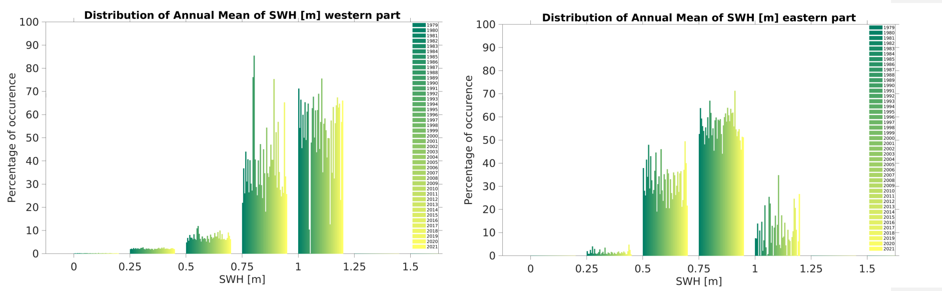

Figure 28: Histograms of the annual mean of the significant wave height (x-axis, in metres) for the whole Black Sea and additionally for the western and eastern part for the years 1979-2021 (lower row).

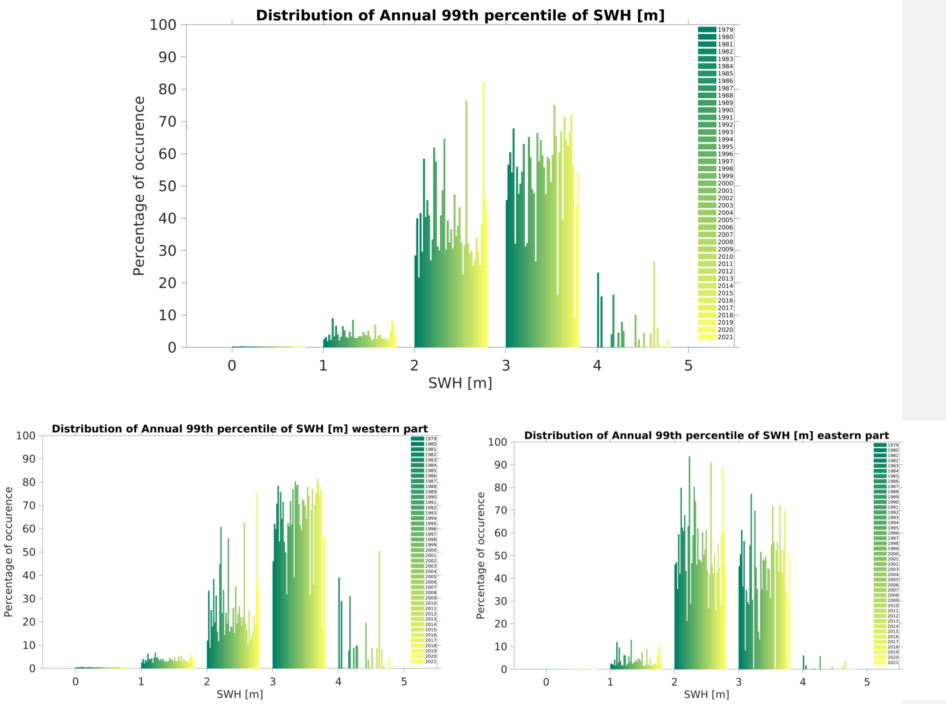

Figure 29: Histograms of the 99th percentile of the significant wave height (x-axis, in metres) for the whole Black Sea and additionally for the western and eastern part for the years 1979-2021 (lower row).

In a new and very interesting depiction, the histograms in the Figure 28 and 29 show the distribution of the annual mean of the significant wave height for the whole Black Sea; additionally also for the western and eastern part of the basin (Figure 28) and the corresponding 99th percentiles (Figure 29). The annual mean for each of the years for the period 1979 – 2021 is distributed over the bins 2-5 in Figure 28 (upper row). Here the height of the individual columns in each of the bins indicate how many events or how many model grid points with proper values occur within the particular bins. The individual columns for each of the years are colour-coded, starting with dark green in 1979 and ends with bright yellow in 2021. The histogram demonstrates the frequency distribution per year and the variability over the years. While in the first bin 0 – 0.25 m there a very few values only, the number of occurrences increase continuously from the first bin to the fourth bin 0.75 – 1 m, in which more than 50% of the annual means for all years are enclosed. As an example (in Figure 28), some years (e.g. 2019) are unusual compared to the other columns. The values are much lower in the fifth bin compared to the forth. Therefore, it is obvious that the highest wave heights are definitely lower in these years compared to all the other years.

The lower row of Figure 28 shows the same histograms separated for the western and the eastern part of the Black Sea. The differences between the occurrences in the particular bins are quite significant. While for the western part, most of the occurrences can be found in the fifth bin in the eastern part of the Black Sea much less values are in this bin. Here most of the means occur in the fourth. That is a clear proof that the mean wave heights are significantly higher in the western part compared to the eastern part of the Black Sea.

The presentation of the values for the annual 99th percentile for the significant wave heights for the period 1979 – 2021 in Figure 29 supports the findings above, although the scatter of the occurrences for the individual years is higher as the one given in Figure 28. Furthermore, in this case the occurrences are distributed over five bins up to 5 m. In the last bin from 4 – 5 m the big storm in 2012 appears in the upper row, and in the plot for the western part of the Black Sea in the lower row on the left.

V.3 Differences of western and eastern basin

With the significant wave height metrics in Figure 30, the different behaviour of the median, the mean and the maximum of the wave height as well as selected percentiles, has been investigated additionally for the western and the eastern part of the Black Sea. All values discussed here are averaged in space. The borderline between the western and the eastern part is defined as the longitude 34°W, as suggested by the second EOF of the significant wave height in (not shown). The curves for the western and the eastern part of the Black Sea have been compared with that one for the complete area. It is obvious that the curves for the median and the mean of the significant wave height differ significantly. The wave heights in the western part are always higher than those generated for the eastern part. The maximum for the median in the western part is 0.88 m and 0.74 m for it the eastern part. For the mean of the significant wave height, the values are higher with 1.05 m for the western part and 0.90 m in the eastern part.

The maximum of the wave height for the period 1979 – 2021 in general is not much higher in the western part of the Black Sea. One of the few deviations of the eastern and western maximum is 1999 in which the eastern part has higher values.

Concerning the percentiles, it turns out that with increasing percentile, the differences between the western and eastern basins decrease. Finally, the differences between the averages of the significant wave heights in the western and eastern parts of the Black Sea can be explained by the different number of storms, the power of the storms, and the area that is covered by those.

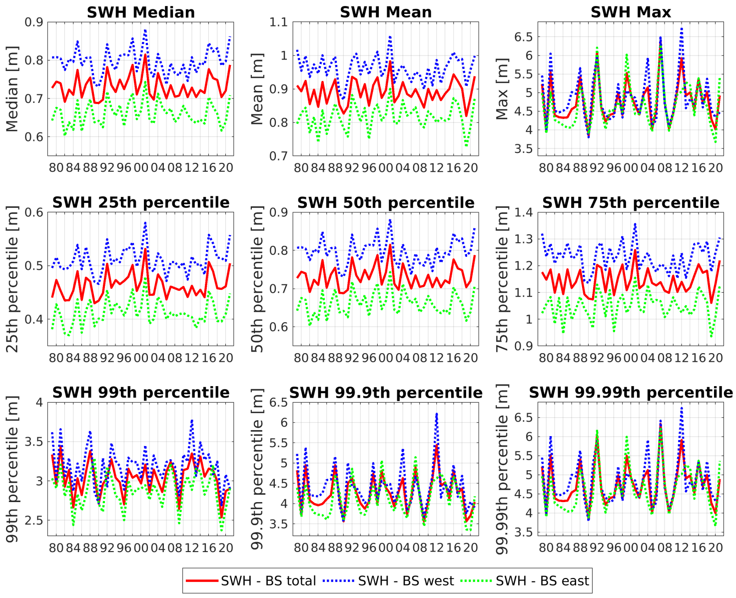

Figure 30: Yearly values of significant wave height metrics for the Black Sea derived from WAM model data shown for the whole basin (red line) as well as for the western (blue dashed line) and the eastern basin (green dashed line). The values are averaged in space. The western and eastern basin are separated at 34°W.

Investigating the maximum values in Figure 31 instead of the averaged values in Figure 30, the significant wave heights are higher of course and the differences for median, mean, maximum and the percentiles in the middle row of Figure 31 are less significant. The curves of the 25th, 75th and 99th percentiles are more similar now. The overall maximum of the significant wave height detected in the Black Sea during the period from 1979 to 2021 is 9.20 m in 2007. That is valid for both the wave height in the western and the eastern part since that event took place exactly on the borderline between the two different basins.

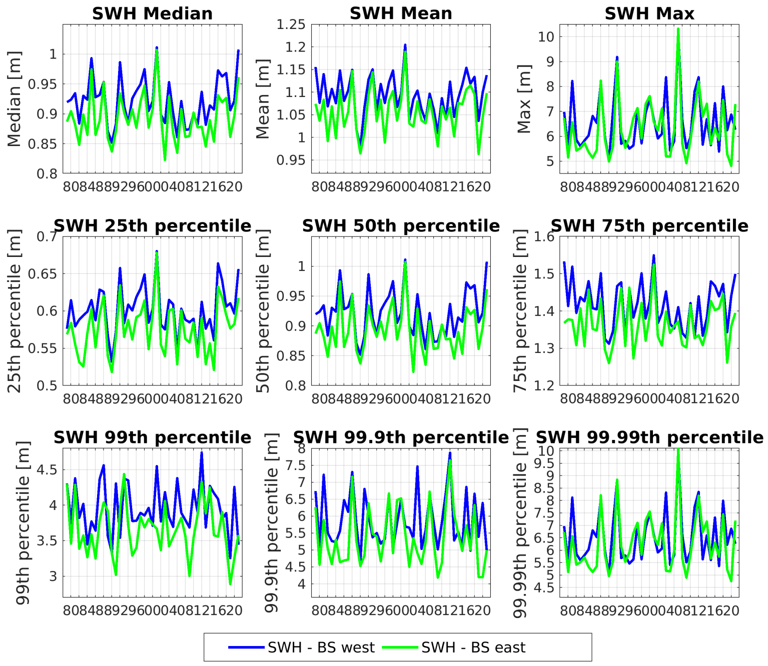

Figure 31: Yearly values of significant wave height metrics for the Black Sea derived from WAM model data shown for the western (blue line) and the eastern basin (green line). In contrast to Figure 30, the maximum values are shown.

V.4 Climatology

Figure 32 and 33 show the monthly climatologies for significant wave height (Figure 32) and Tm02 period (Figure 33).

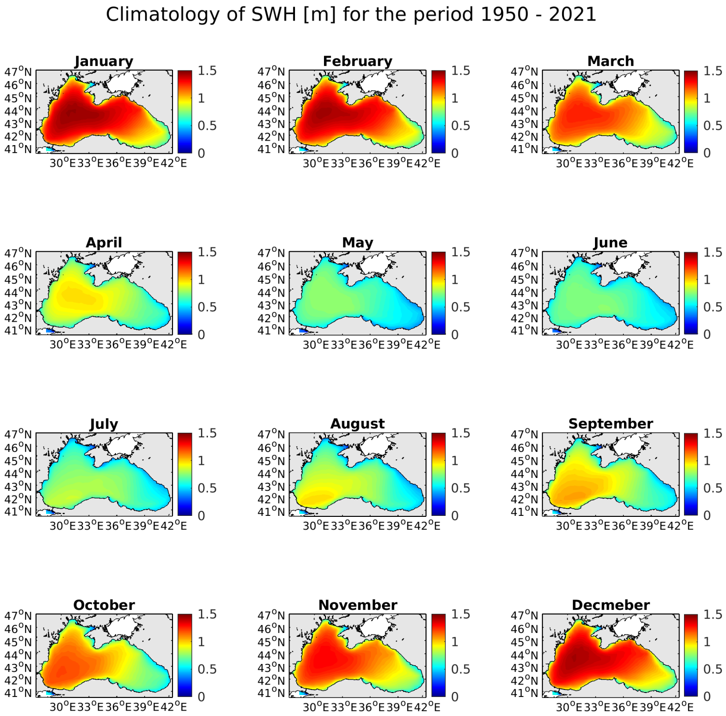

Figure 32: Monthly climatology of the MY product for significant wave height based on the period 1950 to 2021.

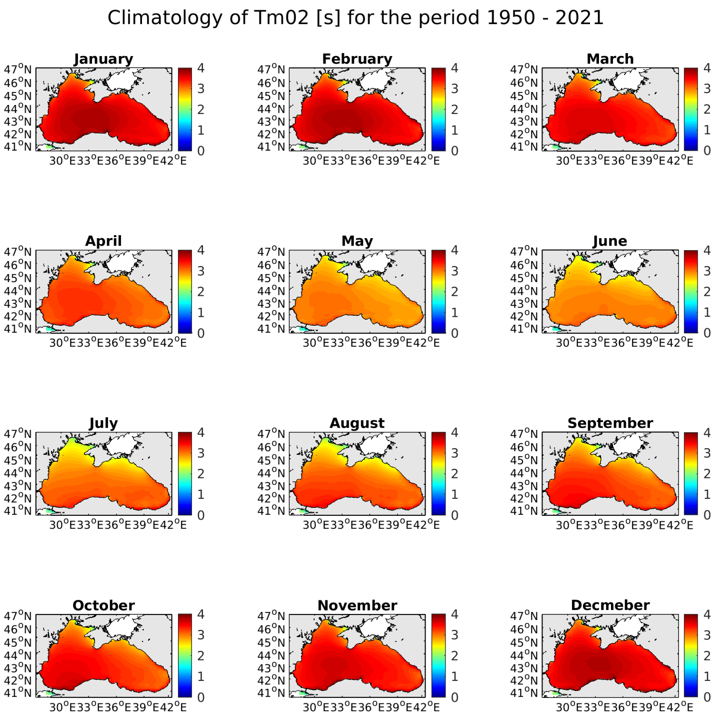

Figure 33: Monthly climatology of the MY product for Tm02 period based on the period 1950 to 2021.

VI SYSTEM'S NOTICEABLE EVENTS, OUTAGES OR CHANGES

The old reanalysis BLKSEA_REANALYSIS_WAV_007_006 has been replaced by the new version of the reanalysis BLKSEA_MULTIYEAR_WAV_007_006 in November 2022.

Future time series extensions are expected to have no related changes in the quality of the product.

Interim datasets are operationally produced on a monthly basis since January 2022 covering the period from the end of the reanalysis dataset until M-1.

Date	Change	Notes
Sep 2019	Release of product	
Dec 2020	New model version	
Jan 2021	Addition of Interim product	
Sep 2021	Addition of the 2020 time series extension	
Nov 2022	MY dataset replaced (new model version WAM - Cycle 6, new model physics - ST4, updated bathymetry, higher horizontal resolution, 2 new maximum wave variables).	
Nov 2023	Addition of time series extension to 1950 and addition of LATEMAR max. variables	

VII QUALITY CHANGES SINCE PREVIOUS VERSION

Beyond all discussions about the quality of the new BS-wave system released in 2022 in the chapters before, a very important question is how the new system performs in comparison to the previous wave routine for the MYP (named "old"). Therefore a couple of plots discussed before have been plotted again, including the old and the new values together in one plot. Starting with the yearly values of significant wave height metrics, shown in Figure 34 which corresponds to the previous Figure 5 in chapter IV.1, it is obvious that all the statistical parameters for the new MYP are slightly worse than those calculated from the model results of the former system. Only the bias has improved. This is due to the new model parameterisations, which aim at optimising the bias. However, the decrease of RMSD (~2 cm) and correlation (0.01) are only of minor importance and the decrease in SI and RV is even smaller. This can be accepted considering the bias improvement of ~3-4 cm for the non-assimilated periods.

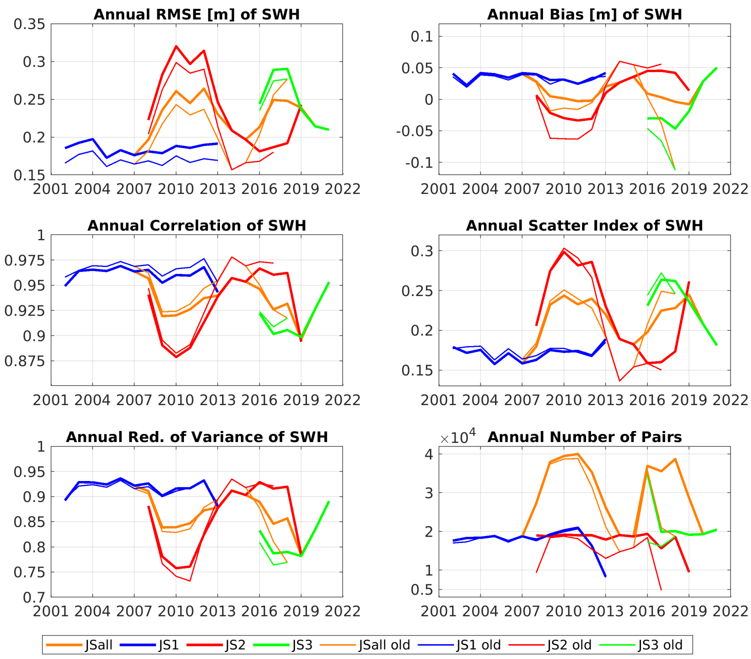

Figure 34: Yearly values of significant wave height metrics for the Black Sea derived from individual and combined satellite measurements in comparison to the previous model version ("old").

The annual time series of the 99th and the 99.9th percentiles for the model and the satellite measurements shown in Figure 35 together with the old curves (corresponding to Figure 6) does also indicate some differences. The differences for the 99th and 99.9th percentiles in the uppermost row demonstrates a reduction of the values up to 20 cm (99th percentile, 2013, JS2) for the new MYP especially during non-assimilated periods. This reveals another model model performance improvement in addition to the bias reduction. The 99th and 99.9th percentiles have increased by about 10 and 30 cm, respectively, compared to the previous system (middle and lower row).

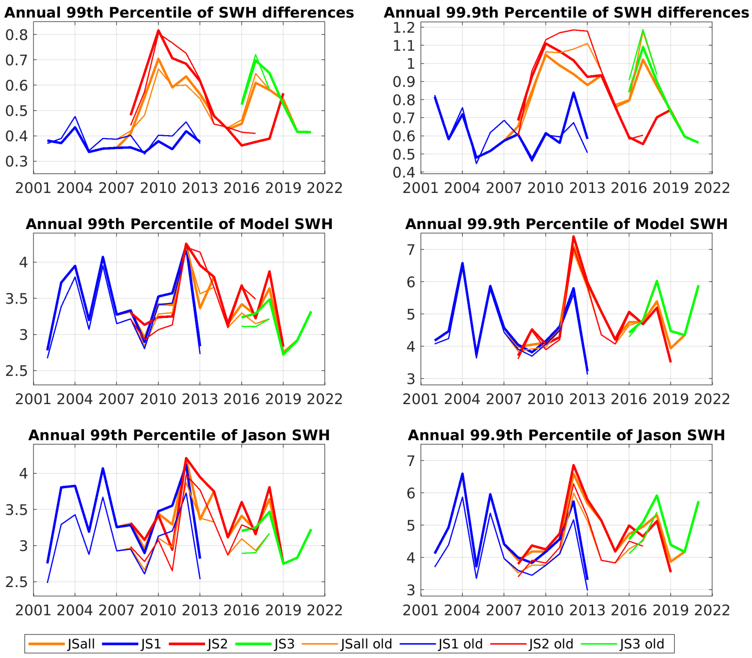

Figure 35: Yearly values of the 99th and 99.9th percentiles of the wave model significant wave heights (middle row), all Jason-data derived from individual and combined satellite measurements (lowermost row) and the differences between both (uppermost row), in comparison to the previous model version ("old").

Figure 36 includes the time series for the annual median and the annual mean of the significant wave height for the model (upper row) and those for the satellite data (lower row). Both quantities show an increase of about 10 cm, which is also present in the satellite data. The increase in the model data is related to the new model parameterisations and in the satellite data to the related quality control of model and satellite data pairs.

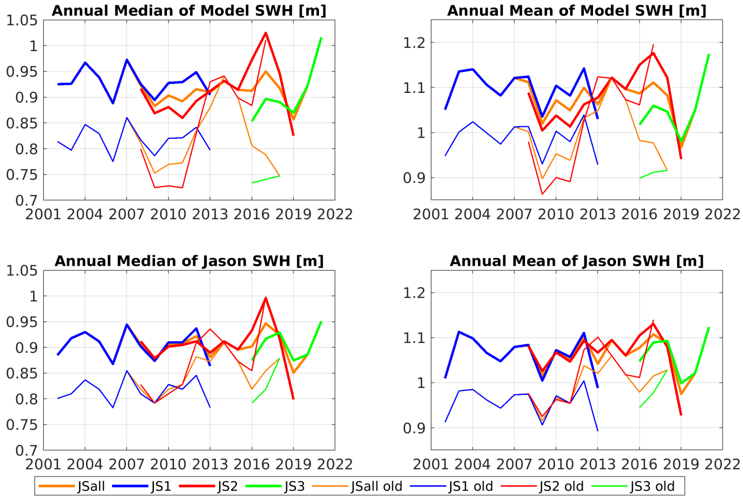

Figure 36: Time series of the annual median and the mean of the significant wave heights along the satellite tracks shown for the wave model (upper row) and the satellite data (lower row) in comparison to the previous model version ("old").

The time series of the annual standard deviation and the annual maximum of the significant wave heights for the model results in the upper row of Figure 37 show only small differences among the old and new model. In contrast, the satellite data in the lower row show an increase of both quantities, which is related to differences in the quality control, which now lead to more realistic standard deviations and maximum values (compare the lower row with the upper row).

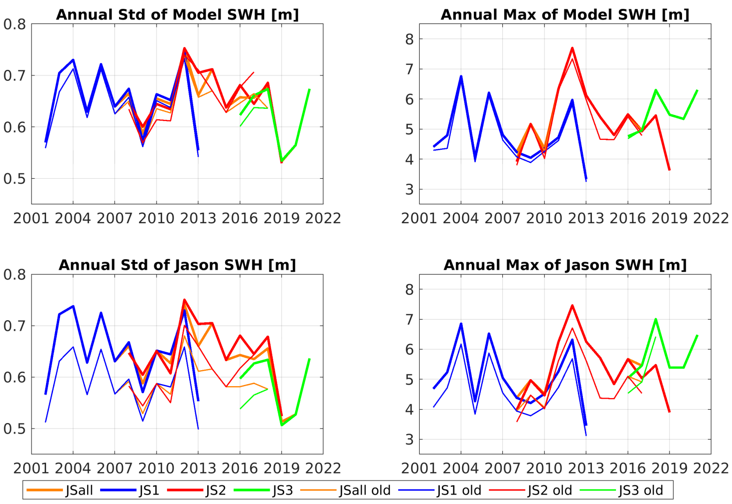

Figure 37: Time series of the annual standard deviation and the maximum of the significant wave heights along the satellite tracks shown for the wave model (upper row) and the Jason-satellite data (lower row) in comparison to the previous model version ("old").

Such comparisons of model and satellite quantities are deeper analysed in the following. Figure 38 shows time series of different metrics, like the median, mean, maximum, and specific percentiles of significant wave height (see also Figure 21). The time series related to the new model (upper figures) can be directly compared with the results of the previous model (lower figures). The main outcome of this comparison is that the model and satellite curved are much better aligned with each other in the new model. In the old model, the WAM results often overestimate the satellite results. Even years, which were difficult to simulate (e.g. 2018) are now much better represented. Furthermore, the significant wave heights have increased in general in the new setup and especially the higher percentiles are better met than in the previous system.

The time series extension to 1950 and the addition of variables in 2023 have no impact on the product quality.

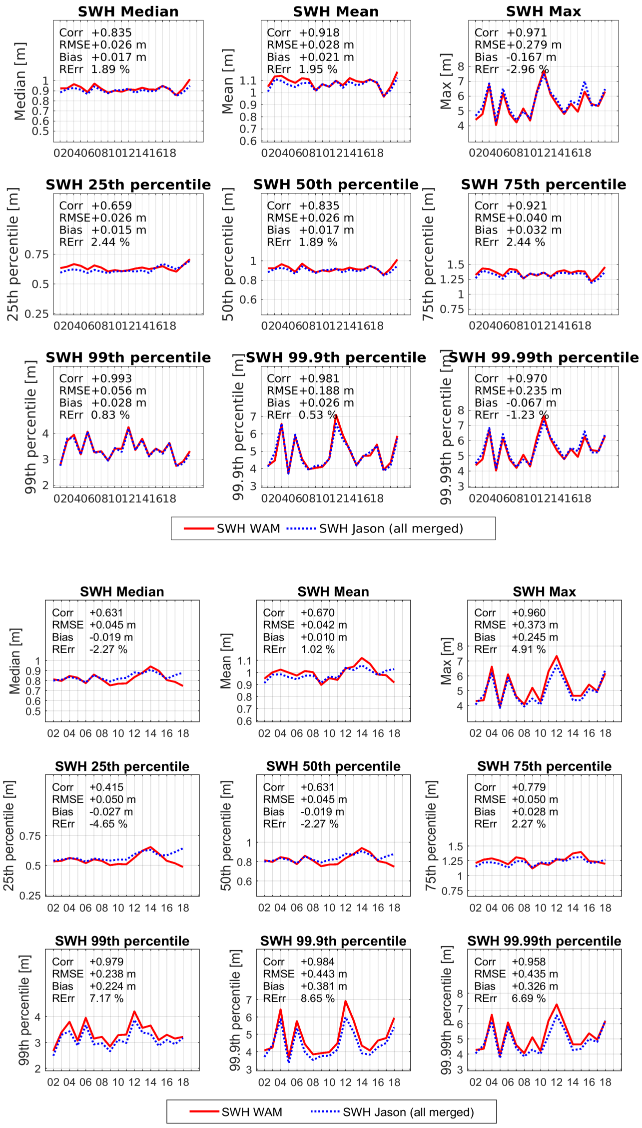

Figure 38: Time series of annual median, mean, and maximum of the significant wave heights, as well as time series of specific annual quantiles of significant wave heights derived from all Jason satellite measurements and from WAM. Upper figures: new model, lower figures: previous model version.

VIII REFERENCES

Chawla A, Spindler DM, Tolman HL (2013) Validation of a thirty year wave hindcast using the Climate Forecast System Reanalysis winds, Ocean Modelling, 70, pp 189-206, doi: 10.1016/j.ocemod.2012.07.005.

ECMWF (2020) IFS Documentation CY47R1, Book Chapter, ECMWF.

Günther H, Hasselmann S, Janssen PAEM (1992) The WAM Model Cycle 4.0. User Manual. Technical Report No. 4, Deutsches Klimarechenzentrum, Hamburg, Germany. 102 pages.

Janssen, P. A. E. M. (1991). Quasi-linear Theory of Wind-Wave Generation Applied to Wave Forecasting. *Journal of Physical Oceanography*, 21(11), 1631-1642. https://doi.org/ 10.1175/1520-0485(1991)021<1631:QLTOWW>2.0.CO;2

Janssen PAEM (2008) Progress in ocean wave forecasting. J Comput Phys 227:3572-3594.

Komen GJ, Cavaleri L, Donelan M, Hasselmann K, Hasselmann S, Janssen PAEM (1994) Dynamics and Modelling of Ocean Waves, Cambridge University Press.

Staneva, J., A. Behrens and Wahle K., (2015) Wave modelling for the German Bight coastal-ocean predicting system, Journal of Physics: Conference Series, 633, pp 233-254, doi:1211, 0.1088/1742-6596/633/1/012117, ISBN: 978-3-939230-28-1

Staneva J, Alari V, Breivik O, Bidlot J-R, Mogensen K (2016a) Effects of wave-induced forcing on a circulation model of the North Sea. Ocean Dynamics, DOI 10.1007/s10236-016-1009-0

Staneva J, Wahle K, Koch W, Behrens A, Fenoglio-Marc L, Stanev E (2016b) Coastal flooding: impact of waves on storm surge during extremes – a case study for the German Bight, Nat. Hazards Earth Syst. Sci., 16, 2373-2389, doi:10.5194/nhess-16-2373-2016Staneva,

Stanev, E.V., Y. He, J. Staneva and E. Yakushev (2014) Mixing in the Black Sea detected from the temporal and spatial variability of oxygen and sulfide – Argo float observations and numerical modelling. Biogeosciences, 11, 5707–5732

von Schuckmann, K. et al. (2020). Copernicus Marine Service Ocean State Report, Issue 4. Journal of Operational Oceanography, 13(sup1), S1–S172. https://doi.org/10.1080/1755876X.2020.1785097

von Schuckmann, K. et al. (2021). The CMEMS Ocean State Report, issue 5, Journal of Operational Oceanography, 14:sup1, s1–s185; DOI: 10.1080/1755876X.2021.1946240

Wahle K., Staneva J., Guenther H., (2015) Data assimilation of ocean wind waves using Neural Networks. A case study for the German Bight, Ocean Modelling, pp. 117-125

WAMDI Group (1988) The WAM model - A third generation ocean wave prediction model. Journal of Physical Oceanography, 18, 1775-1810.